ISTANBUL TECHNICAL UNIVERSITY ★ GRADUATE SCHOOL

PACK ALUMINIZING OF A COBALT-BASED SUPERALLOY

M.Sc. THESIS

İlknur KARA

Department of Metallurgical and Materials Engineering

Production Metallurgy and Technologies Engineering Programme

MAY 2025

ISTANBUL TECHNICAL UNIVERSITY ★ GRADUATE SCHOOL

PACK ALUMINIZING OF A COBALT-BASED SUPERALLOY

M.Sc. THESIS

İlknur KARA
(506211217)

Department of Metallurgical and Materials Engineering

Production Metallurgy and Technologies Engineering Programme

Thesis Advisor: Prof. Dr. Murat BAYDOĞAN

MAY 2025

ISTANBUL TEKNİK ÜNİVERSİTESİ ★ LİSANSÜSTÜ EĞİTİM ENSTİTÜSÜ

KOBALT ESASLI BİR SÜPERALAŞIMIN KUTU ALÜMİNYUMLAMA İŞLEMİ

YÜKSEK LİSANS TEZİ

İlknur KARA
(506211217)

Metalurji ve Malzeme Mühendisliği Anabilim Dalı

Üretim Metalurjisi ve Teknolojileri Mühendisliği Programı

Tez Danışmanı: Prof. Dr. Murat BAYDOĞAN

MAYIS 2025

Ilknur KARA, a M.Sc. student of İTU Graduate School student ID 506211217, successfully defended the thesis entitled “PACK ALUMINIZING OF A COBALT-BASED SUPERALLOY”, which she prepared after fulfilling the requirements specified in the associated legislations, before the jury whose signatures are below.

Thesis Advisor :	**Prof. Dr. Murat BAYDOĞAN** İstanbul Technical University	.....
Jury Members :	**Prof. Dr. Hüseyin ÇİMENOĞLU** Istanbul Technical University	.....
	Dr. Hadi JAHANGİRİ Koç University	.....

Date of Submission : 5 May 2025
Date of Defense : 29 May 2025

To my family,

FOREWORD

I would like to thank Prof. Dr. Murat BAYDOĞAN for his guidance and extraordinary support in this research project.

My sincere gratitude to Şencan ÖZKAN, Burak EVREN, İbrahim BERBER, Berkay DEMİRCAN and all BAYKAR Materials Development team members for their great supports during my experimental studies.

Furthermore, I extend my thanks to Res. Assist. Erdem BALCI from ITU Metallurgical and Materials Engineering for his valuable support.

I also would like to thank my beloved family for their endless support and uncontidional love.

May 2025

İlknur KARA
(Metallurgy and Materials Engineer)

TABLE OF CONTENTS

Page

FOREWORD ..... **ix**
TABLE OF CONTENTS ..... **xi**
ABBREVIATIONS ..... **xiii**
SYMBOLS ..... **xv**
LIST OF TABLES ..... **xvii**
LIST OF FIGURES ..... **xix**
SUMMARY ..... **xxi**
ÖZET ..... **xxiii**
1. INTRODUCTION **1**
2. SUPERALLOYS **3**
2.1 Cobalt Based Superalloys 5
2.2 Coatings For Superalloys and High Temperature Applications 9
2.2.1 Diffusion aluminide coatings 10
2.2.1.1 Pack aluminizing process 11
2.2.1.2 Above pack process 13
2.2.1.3 Chemical vapor deposition method 13
3. EXPERIMENTAL DETAILS **15**
3.1 Material 15
3.2 Heat Treatment Procedures 15
3.3 Pack Aluminizing Procedure 16
3.4 Microstructural Characterization 16
3.5 Mechanical Characterization 17
3.5.1 Hardness test 17
4. RESULTS AND DISCUSSIONS **19**
4.1 Process Design of Homogenization 19
4.2 Microstructural Characterization 20
4.2.1 Microstructure of received material 20
4.2.2 Post homogenization microstructure 23
4.2.3 Carbide volume fraction and hardness calculations 24
4.2.4 Post pack aluminizing microstructure 25
4.2.5 As cast and homogenized sample's microstructure after aluminizing 33
4.2.6 Microstructures of aluminizing after different surface preparations 34
4.3 Coating hardness test 35
5. CONCLUSIONS AND RECOMMENDATIONS **37**
REFERENCES **39**
CURRICULUM VITAE **45**

ABBREVIATIONS

CVD	**:** Chemical Vapor Deposition
EDS	**:** Energy Dispersive Spectroscopy
FCC	**:** Face-centered Cubic
HTLA	**:** High Temperature Low Activity
LTHA	**:** Low Temperature High Activity
SEM	**:** Scanning Electron Microscopy

SYMBOLS

γ'	: Ni_3Al phase
γ''	: Ni_3Nb phase

LIST OF TABLES

Page

Table 2.1 : Effect of some alloying elements on superalloys..... **4**
Table 2.2 : Effects of alloying elements on cobalt alloys' properties..... **7**
Table 2.3 : Carbide types and the elements they contain **7**
Table 2.4 : Examples of aluminide pack compositions..... **12**
Table 3.1 : Chemical composition of the cobalt-based superalloy (wt.%) **15**
Table 3.2 : Homogenization conditions applied **15**
Table 4.1 : At. % Co and Al composition of each layer and substrate **27**
Table 4.2 : Chemical composition (at.%) of structures indicated in Figure 4.9 ..... **29**
Table 4.3 : Hardness and elastic behavior of each coating layer **36**

LIST OF FIGURES

Page

Figure 2.1 : Stress- rupture behavior of different superalloy groups **5**
Figure 2.2 : Carbide and dislocation interaction of Haynes 188 alloy after creep test (927 °C/ 41.4 MPa)..... **6**
Figure 2.3 : Schematic figure of oxidation of WI-52 cobalt-based superalloy..... **8**
Figure 2.4 : High temperature coatings and their relative coating life and temperature enhancement **9**
Figure 2.5 : Different diffusion coating methods..... **11**
Figure 2.6 : Schematic image of chemistry in the pack aluminizing process..... **11**
Figure 2.7 : Schematic image of the pack process **12**
Figure 2.8 : Schematic image of above-pack process..... **13**
Figure 2.9 : Schematic diagram of a) above-pack process and b) CVD process where the aluminide halides generated externally..... **14**
Figure 4.1 : Temperature dependent change of volume fraction of phases for the alloy used in this study **19**
Figure 4.2 : Optical micrographs in different magnifications (a,b) and SEM (c) micrograph of the as received sample (as-polished)..... **21**
Figure 4.3 : EDS mapping analysis of as received sample **22**
Figure 4.4 : Optical micrograph of as received sample (a), optical micrographs and SEM images of HT-1200-1 (b,e,h), HT-1250-1 (c,f,i) and HT-1250-10 (d,g,j) samples..... **24**
Figure 4.5 : (a) Carbide volume fraction and hardness change of different conditions, (b) Hardness and carbide volume fraction dependency **25**
Figure 4.6 : Coating microstructure of as-cast sample..... **26**
Figure 4.7 : Matrix composition of substrate (b) and each coating layer, thin layer (c), interdiffusion layer (d), mid layer (e), outer layer dark gray (f) and outer layer light gray (g) **28**
Figure 4.8 : Coating micrographs of as-cast sample in different magnifications **29**
Figure 4.9 : EDS analysis of precipitates found in coating microstrusture..... **30**
Figure 4.10 : EDS mapping of coating microstructure. **31**
Figure 4.11 : EDS line analysis of coating microstructure **32**
Figure 4.12 : XRD analysis of coated specimen **32**
Figure 4.13 : Microstructure of the coated sample **33**
Figure 4.14 : (a-c-e-g) Microstructures of as-cast+ aluminide coated and (b-d-f-h) Microstructures of homogenized+ aluminide coated samples **34**
Figure 4.15 : Coating thickness distributon after different surface preparation conditions..... **35**

PACK ALUMINIZING OF A COBALT-BASED SUPERALLOY

SUMMARY

Cobalt-based superalloys manufactured by casting are used in applications with corrosive environments, under high temperature and relatively moderate-low loads. Components manufactured from these alloys are expected to exhibit high thermal stability; thermal fatigue, creep and hot corrosion resistance. Cobalt-based superalloys contain several alloying elements and as a result, segregation is encountered in the structure. Segregation leads to the formation of undesirable phases in the microstructure and thus adversely affects the mechanical properties. In order to eliminate the negative effects of segregation in materials manufactured by casting, homogenization heat treatment is performed. This process is based on the principle of diffusion of alloying elements under certain temperatures and times.

Cobalt based superalloys are used in such applications that corrosion environment is severe. The cobalt-formed CoO layer lacks protective properties; hence, various coatings are employed to mitigate oxidation and hot corrosion. The most widely used of these coatings for a long time are aluminide coatings. Aluminide coatings are currently applied by Pack aluminizing and chemical vapour deposition methods. Aluminide coatings increase the resistance against oxidation and hot corrosion thanks to the protective Al_2O_3 layer they form on the material surface.

In this study, homogenization and pack aluminizing processes at different conditions were applied to a cobalt-based superalloy, which has been used as turbine stator material in the gas turbine engine industry for many years.

Homogenization conditions were determined with the assistance of ThermoCalc software and carried out in three different conditions: 1 hour at 1200 °C, 1 hour at 1250 °C and 10 hours at 1250 °C. After homogenization, the samples were cooled in water. The microstructural changes after homogenization were examined by optical microscopy and scanning electron microscopy (SEM). Energy Dispersive Spectrometry (EDS) was used to analyze the chemical composition changes of each phase and hardness changes were analyzed. The morphological changes of carbides, which are the structure of the casting and the main strengthening mechanism, were examined and the changes in the carbide volume fraction were observed with the help of Image J program.

Pack aluminizing aluminide coating conditions were determined with the help of the literature. Pre-process surface preparations were carried out under different conditions and their effect on the coating structure was observed. Coating microstructure, thickness and unifomity were examined by optical microscope and scanning electron microscope (SEM), and Energy Dispersive Spectrometry (EDS) was used to analyse the chemical composition of the formed phases.

It was observed that as the homogenization times and temperatures increased, the carbide morphologies changed from the initial continuous and chinese script

morphology to discontinuous, thin and spherical morphology, the carbide ratio and therefore the hardness of the material decreased, but there was no significant change in the chemical composition of the carbide phases. It was determined that the dentritic structure existing after casting was eliminated especially after homogenization at 1250 °C for 10 hours.

Pack aluminizing coating was carried out at 1040 °C for 4 hours to both as cast and homogenized samples based on the literature. The same coating structure was formed in both conditions. Coating thicknesses up to 290 μm were observed, but the thickness distribution was uneven, especially at the corners of the sample, no coating layers were observed. There was no phase transformation in the substrate material after coating. After coating, an aluminide coating structure with four layers was obtained. A thin transition layer with a thickness of about 2 μm was formed just above the base material. This thin layer has a sawtooth morphology and is strongly adhered to the substrate. Above this layer, an interdiffusion layer with a thickness of about 21 μm and a middle layer with a thickness of 20 μm were observed. In these three layers, fine $(Cr,W)_{23}C_6$ carbides are homogeneously distributed. The outer layer was 240 μm thick and accounted for about 85% of the coating thickness. It was observed that $(Cr,W)_{23}C_6$ carbides were absent in this layer, but NbC carbides present in the base material persisted throughout the coating. Al_2O_3 structures and cratered horizontal cracks were also observed. A columnar structure was observed at the very outside of the coating. In order to homogenize the coating thickness across the entire cross-section, coating trials were carried out on the surfaces after polished, 120 grid sanding and rough cutting. The best results were obtained after polishing, rough cutting, 120 grid sanding and 400 grid sanding, respectively. XRD measurement showed that the coating compound formed was $Al_{13}Co_4$.

KOBALT ESASLI BİR SÜPERALAŞIMIN KUTU ALÜMİNYUMLAMA İŞLEMİ

ÖZET

Kobalt esaslı süperalaşımlar endüstride özellikle yüksek sıcaklık, orta-düşük yük koşulları altında ve korozif ortamlarda kullanılacak parçaların üretiminde kullanılmaktadır. Kobalt esaslı süperalaşımlar gösterdikleri yüksek termal stabilite, sıcak korozyon direnci, sürünme ve termal yorulma direnci gibi özellikleri sayesinde ön plana çıkmaktadır. Bu alaşımlar nikel esaslı süperalaşımlar ile birlikte özellikle gaz türbinli motorların türbin ve yanma bölümlerinde sırasıyla hareketli ve yapısal parçaların üretiminde kullanılır. Gaz türbinli motorlarda kompresör tarafından sıkıştırılan hava yanma odasında yakılarak ortam sıcaklıkları 2000 K'i bulan türbin kısmına iletilir, burada statorlar yanmış gazları doğru açıyla rotorlara iletir ve rotorların dönmesi sağlanır. Stator parçaları hareket etmemesine rağmen çok yüksek termal yüklere maruz kalır. Kobalt esaslı süperalaşımlar stator uygulamalarında 1940'lı yıllardan beri en yaygın kullanılan alaşımlardır.

Nikel esaslı süperalaşımlar kobalt esaslı süperalaşımlara göre daha yüksek mukavemet göstermektedir. Bunun nedeni nikel alaşımlarda katı çözelti sertleşmesi ve karbür çökeltilerinin oluşumunun yanında intermetalik çökeltilerin de oluşması ve mukavemete katkı sağlamasıdır. Bu nedenle hareketli rotor parçalarında nikel esaslı süperalaşımlar kullanılır. Kobalt esaslı süperalaşımlarda ise asıl mukavemetlendirme mekanizması karbür çökeltileridir ayrıca katı çözelti sertleşmesi de mukavemete katkı sağlamaktadır.

Günümüzde kobalt esaslı süperalaşımlar genelde döküm kondisyonunda kullanılırken, çözeltiye alma ve yaşlandırma uygulanan örnekler de bulunmaktadır. Kobalt esaslı süperalaşımlar bünyelerinde farklı fiziksel ve kimyasal özelliklere sahip birçok alaşım elementi barındırır, bu nedenle döküm kondisyonundaki kobalt alaşımları, dökümünün ardından neredeyse kaçınılmaz olarak segregasyon oluşumuyla karşılaşır. Segregasyon, mikroyapıda elementlerin ve fazların homojen dağılmaması olarak tanımlanabilir ve sonucunda zararlı fazlar oluşarak mekanik özellikler olumsuz etkilenir. Segregasyonun giderilmesi için homojenizasyon ışıl işlemi uygulanabilir. Homojenizasyon işleminde malzeme, mikroyapısında yer alan çökeltilerin tamamen çözünerek aşırı doymuş bir matris yapısı oluşturacağı yüksek bir sıcaklığa ısıtılır. Burada dikkat edilmesi gereken en önemli husus alaşımın maruz kalacağı sıcaklığın solidüs sıcaklığının altında olmasıdır. Homojenizasyon işlemi sırasında mikroyapıda lokal ergimelerin gerçekleşmesi daha çok segregasyon ve hatta gözenek oluşumuna neden olabilmektedir. Homojenizasyona tabi tutulacak malzeme bu sıcaklığa ulaştıktan sonra belli bir süre bu sıcaklıkta tutulmalı ardından tekrar çökelmeye mahal vermeyecek bir hızda soğutulmalıdır. Soğutma; havada, suda veya yağda gerçekleştirilebilmektedir.

Kobalt esaslı süperalaşımların kullanıldığı sıcaklıklarda oksidasyon ve sıcak korozyona karşı önlem almak amacıyla farklı kaplamalar kullanılmaktadır, kobaltın

oluşturduğu CoO tabakası koruyucu değildir ve belli sıcaklıkların üzerinde yüksek hızla malzemenin merkezine doğru ilerler. Bu kaplamalardan uzun süredir en yaygın olarak kullanılanı alüminat kaplamalardır. Alüminat kaplamalar günümüzde kutu alüminyumlama ve kimyasal buhar biriktirme yöntemleriyle uygulanmaktadır. Alüminat kaplamalar, malzeme yüzeyinde oluşturdukları koruyucu Al_2O_3 katmanı sayesinde oksidasyona ve sıcak korozyona karşı direnci arttırmaktadır.

Bu çalışmada uzun yıllardır gaz türbin motorları endüstrisinde türbin stator malzemesi olarak kullanılan kobalt esaslı bir süperalaşıma farklı koşullarda homojenizasyon ve kutu alüminyumlama işlemleri uygulanmıştır.

Homojenizasyon koşulları ThermoCalc yazılımı yardımıyla belirlenmiş, 1200 °C'de 1 saat, 1250 °C'de 1 ve 10 saat olmak üzere üç farklı koşulda gerçekleştirilmiştir. Homojenizasyon sonrası numuneler suda soğutulmuştur. Homojenizasyon işlemi sonrasında gerçekleşen mikroyapı değişimleri, optik mikroskop ve taramalı elektron mikroskobu (SEM) ile incelenmiştir. Her bir fazın kimyasal bileşim değişiminin analizi için Enerji Dağılım Spektrometresi (EDS) kullanılmış ve sertlik değişimleri incelenmiştir. Döküm yapısı ve ana mukavemetlendirme mekanizması olan karbürlerin morfolojik değişimleri incelenmiş, Image J programı yardımıyla karbür hacim oranındaki değişim belirlenmiştir.

Kutu alüminyumlama koşulları belirlenirken literatürden yardım alınmış ve proses 1040 °C'de 4 saat gerçekleştirilmiştir. Proseste %70 Al_2O_3, %25 Al ve %5 Al_3Cl kimyasal bileşimine sahip paketler kullanılmış, kaplama numunelerin bu paketlere gömülmesinin ardından gerçeklştirilmiştir. Proses öncesi yüzey hazırlıkları parlatılmış, kaba kesme sonrası ve farklı zımparalama koşulları olmak üzere farklı koşullarda gerçekleştirilmiş ve kaplama yapısı ile kaplama kalınlık dağılımına olan etkisi gözlemlenmiştir. Kaplama mikroyapısı, kalınlığı ve homojenliği optik mikroskop ve taramalı elektron mikroskobu (SEM) ile incelenmiş, oluşan fazların kimyasal bileşim değişiminin analizi için Enerji Dağılım Spektrometresi (EDS) kullanılmıştır. Ayrıca nanoindentasyon yöntemiyle her bir kaplama tabakasının sertliği ölçülmüştür.

Homojenizasyon süreleri ve sıcaklıkları arttıkça karbür morfolojilerinin başlangıçtaki sürekli ve çin yazısı morfolojisinin; süreksiz, ince ve küresel morfolojiye döndüğü, karbür oranının ve dolayısıyla malzemenin sertliğinin azaldığı, ancak karbür fazlarının kimyasal bileşiminde önemli bir değişim olmadığı gözlemlenmiştir. Homojenizasyon öncesi malzeme sertlği 36 HRC olarak belirlenmiştir. 1200 °C'de 1 saat ısıl işlemin ardından karbür miktarında ve sertlikte önemli bir değişim gözlenmemiştir (35 HRC). 1250 °C'de 1 saat ısıl işlem sonrasında döküm kondisyonun % 6 olan karbür miktarının % 3'e, sertliğin ise 30 HRC'ye düştüğü saptanmıştır. 1250 °C'de 10 saat ısıl işlem yapılan numunelerde ise karbür miktarı % 2, sertlik ise 27 HRC olarak belirlenmiştir. Bu ısıl işlem sonrasında $(Cr,W)_{23}C_6$ karbürleri tamamen çözünürken NbC karbürleri Çin yazısı morfolojisinden küresel, ince ve homojen dağılmış morfolojiye dönüşmüştür. ThermoCalc hesaplamalarından da beklendiği üzere NbC karbürler tamamen çözünmemiştir. Döküm sonrası var olan dentritik yapının ise özellikle 1250 °C'de 10 saat yapılan homojenizasyonun ardından giderildiği belirlenmiştir. Karbür miktarı ve malzeme sertliğinin doğru orantılı olarak azaldığı gözlemlenmiştir.

Kutu alüminyumlama işlemi homojenizasyon ve döküm koşullarındaki numunelere uygulanmıştır, kaplama öncesi numuneler 400 grit zımpara kağıdı ile zımparalanmıştır. Her iki koşulda da aynı kaplama yapısı oluşmuştur. Kaplama

kalınlığı literatürde aynı alaşım ve proses için görülen 60 µm kalınlığının aksine tersine 290 µm kalınlıkta elde edilmiştir. Ancak kalınlığın değişken olduğu, özellikle numune köşelerinde kaplama katmanlarının oluşmadığı gözlemlenmiştir. Kaplama sonrası altlık malzemede herhangi bir faz dönüşümü gerçekleşmemiştir. Kaplama sonrasında dört katmana sahip alüminat kaplama yapısı elde edilmiştir. Altlık malzemenin hemen üstünde yaklaşık 2 µm kalınlığında ince bir geçiş tabakası oluşmuştur. Bu ince tabaka testere dişi morfolojisine sahiptir ve altlık malzemeye iyi bir şekilde tutunmuştur. Bu tabakanın üzerinde yaklaşık 21 µm kalınlığında interdifüzyon tabakası ve 20 µm kalınlığında orta katman gözlemlenmiştir. Bu üç katmanda ince $(Cr,W)_{23}C_6$ karbürleri homojen bir şekilde dağılmıştır. Dış katman 240 µm kalınlığındadır ve kaplama kalınlığının yaklaşık % 85'ini oluşturmaktadır. Bu katmanda $(Cr,W)_{23}C_6$ karbürlerinin bulunmadığı ancak altlık malzemede bulunan NbC karbürlerin devam ettiği görülmüştür. Ayrıca Al_2O_3 yapılarına ve yer yer krater halini almış yatay çatlaklara da rastlanmıştır. Kaplamanın en dışında kolonsal yapı gözlemlenmiştir. Kaplama kalınlığını tüm kesit boyunca homojen hale getirmek için parlatılmış, 120 grit zımpara ve kaba kesme sonrası yüzeylere kaplama denemesi yapılmıştır. En iyi sonuçlar sırasıyla parlatılmış, kaba kesme sonrası, 120 grit zımpara ve 400 grit zımpara sonrasında alınmıştır. XRD analizi oluşan kaplama bileşiğinin $Al_{13}Co_4$ olduğunu göstermiştir. Kaplama katmanlarının sertliği nanoindentasyon metodu ile ölçülmüş, altlık malzeme sertliğine oranla tüm kaplama katmanlarının yüksek sertlik gösterdiği görülmüştür. İnterdifüzyon tabakasının sertliği 11,5 GPa'ken orta, dış ve en dış kolonsal bölgenin sertliği sırasıyla 12,4, 9,5 ve 9,4 GPa olarak ölçülmüştür.

1. INTRODUCTION

Cobalt-based superalloys are widely used in the manufacturing of structural parts in high temperature regions of gas turbine engines because they maintain their mechanical properties at high temperatures, show high thermal stability and have good corrosion resistance even at high temperatures. These alloys are usually used to manufacture high- and low-pressure turbine stator and sealing parts [1]. WI-52 is a cobalt-based superalloy that demonstrates good creep resistance and oxidation stability, making it suitable for hot-section components. However, under long exposure to aggressive environments, these materials such as WI-52 may suffer from accelerated oxidation and hot corrosion. Therefore, heat treatment and coating processes used in the production of these alloys are being improved by ongoing R&D work [2,3].

Cobalt-based superalloys are generally used in as-cast condition, but segregation after casting may cause the formation of undesirable phases and thus mechanical properties may be adversely affected. In metallic materials homogenization heat treatment can be applied to prevent segregation [4].

Homogenized cobalt-based superalloys have relatively high strength at higher temperatures yet their oxidation and corrosion resistance get lower [5]. In order to prevent oxidation and hot corrosion several coatings are applied to cobalt based superalloys, such as overlay (MCrAlY), thermal barrier coatings, conventional and modified CVD and pack aluminide coatings [6-8]. One surface modification technic is pack aluminizing which is highly used for their easy application. In this method, the substrate is embedded in a powder mixture containing an aluminum aluminum powder, an activator and an inert filler. At temperatures that coating is applied, aluminum is transported in the vapor phase and diffuses into the substrate surface, and forms a protective layer. Aluminide coatings increase the resistance against oxidation and hot corrosion by the protective Al_2O_3 layer formed on the material surface [9,10].

The pack aluminizing process typically results in the formation of Co-Al products which forms with the order of Al_9Co_2, $Al_{13}Co_4$, Al_3Co, Al_5Co_2, AlCo [11,12]. This Co-Al products form the outer coating layer, between the substrate and this coating layer is an interdiffusion layer which $M_{23}C_6$ (M:Cr, W) carbides are precipitated. After heat treatment or operation the outer surface generally forms a dense and adherent alumina (Al_2O_3) scale that provides the primary oxidation barrier [13,14].

In previous studies, coatings with a thickness of approximately 50-60 μm were obtained using packs of different chemical compositions and different process conditions. After these coating high temperature cycling oxidation resistance was improved [9,15]. In this study, 70% Al_2O_3, 25% Al and 5% Al_3Cl pack compositions and different surface preparations (120 grit grinding, 400 grit grinding, post-cut surface and polished surface) were used for pack aluminizing.

In this thesis, homogenization and pack aluminizing aluminide coating processes were applied to a cobalt-based superalloy under different conditions. The microstructure resulting from these processes was examined by optical microscopy and scanning electron microscopy (SEM), Energy Dispersive Spectrometry (EDS) was used to analyse the chemical composition change of the formed phases. Carbide volume fraction and hardness changes were observed after homogenization. After pack aluminizing, XRD analysis was conducted and hardness of each coating layer was measured with nanoindentation method.

2. SUPERALLOYS

The properties of many materials at room temperature are adversely affected at high temperatures dramatically. High temperature applications are encountered in many industries such as the petrochemical industry, power generation and gas turbine engines used in aviation platforms. The feature that makes superalloys of high strategic importance for countries in the last century and makes them one step ahead of other alloys is their relatively high mechanical properties and oxidation/corrosion resistance at temperatures close to melting temperatures [16,17].

In fact, the most critical issue in the development and more efficient operation of aircraft engines is developments in the area of high temperature alloys which are mainly superalloys, used in the turbine section.

The first appearance of superalloys dates back to the industrial revolution. In the early 20th century, the need for heat-resistant materials led to the development of 'high-temperature materials' obtained by adding elements such as Ni, Co and Cr to steel alloys. In the same period, the invention of vacuum melting technology paved the way for superalloys. With the increase in production rates after the industrial revolution, the need for more resistant materials for machining end materials at high temperatures arose, and Elwood Haynes found a solution to this problem with developing Co-Cr alloys. In the same period, A.L. Marsh, who was working on electrical resistance, developed Ni-Cr alloys. Aircraft engines, which are the main area of use of superalloys, have risen with the development of the aviation industry and different superalloys have been developed in many parts of the world [16,18].

Superalloys can be defined as alloys that are composed of base elements such as cobalt, nickel, iron and many other alloying elements. These alloys can maintain their mechanical and oxidation/corrosion properties under high temperature and aggressive environmental conditions. The main alloying elements they contain are light metals such as Al, Ti and refractory metals such as Cr, Ta, Ru, W, Mo, Nb, Re. While light alloying elements form strengthening precipitate phases; refractory alloying elements provide solid solution strengthening by dispersing into the matrix, high thermal

stability due to their low diffusion rates and additional strengthening thanks to the carbide precipitates they form. Cr and Al increase corrosion resistance by forming a protective oxide layer on the surface of the alloy [19]. Effect of mostly used alloying elements on superalloys is summarized in Table 2.1.

Table 2.1 : Effect of some alloying elements on superalloys [2].

Alloy Addition	Solid Solution Strengtheners	γ' former	Carbide Formers	Grain Boundary Strengtheners	Oxide Scale Formers
Cr	X		X		X
Al		X			X
Ti		X	X		
Mo	X		X		
W	X		X		
B				X	
Zr				X	
C				X	
Nb		X	X		
Hf			X	X	
Ta		X	X	X	

Nickel, cobalt and iron based superalloys are widely used in structural and rotor hot zone (turbine, combustion chamber, afterburner) parts of gas turbine engines. These alloys can be manufactured by casting, forging, rolling, powder metallurgy and in recent years by additive manufacturing methods. Their development is enabled by conducting research and development activities on chemical composition and heat treatment applications. Nickel and cobalt based superalloys can operate under 1300 °C temperatures in the hot zone of gas turbine engines. These temperatures can reach up to 1750 °C with the help of advanced cooling and coating technologies [20].

Iron-based superalloys are widely used in low-pressure turbine and high-pressure compressor parts with relatively low temperatures. In addition to its high iron content, ithese alloys contain about 15-25% nickel. Besides solid solution strengthening, they also gain strength with γ′ (Ni_3Al) and γ′′ (Ni_3Nb) precipitates. The feature that makes this alloy group superior to other superalloys is its lower thermal expansion coefficient. The use of narrow clearance tolerances, especially in aviation engines, has led to the need for low thermal expansion in the materials used. The widespread use of iron-based superalloys is largely due to their low cost [3], [21].

Nickel-based superalloys have an FCC crystal structure and in addition to their solid solution strength thanks to the high amount of alloying elements they contain, can operate under both high load and high temperature, such as turbine blades, by forming a stable and strong structure at high temperatures with the contribution of γ' (Ni_3Al) phase that can be formed by aging heat treatment. Nickel-based superalloys are the largest and most widely used group of superalloys [22,23]. The stress-rupture behavior of iron, nickel and cobalt-based superalloys are shown in Figure 2.1.

Cobalt-based superalloys show relatively better corrosion resistance and thermal stability than nickel-based superalloys, but these alloys are used in static parts under relatively medium to low loads due to their low strength [24].

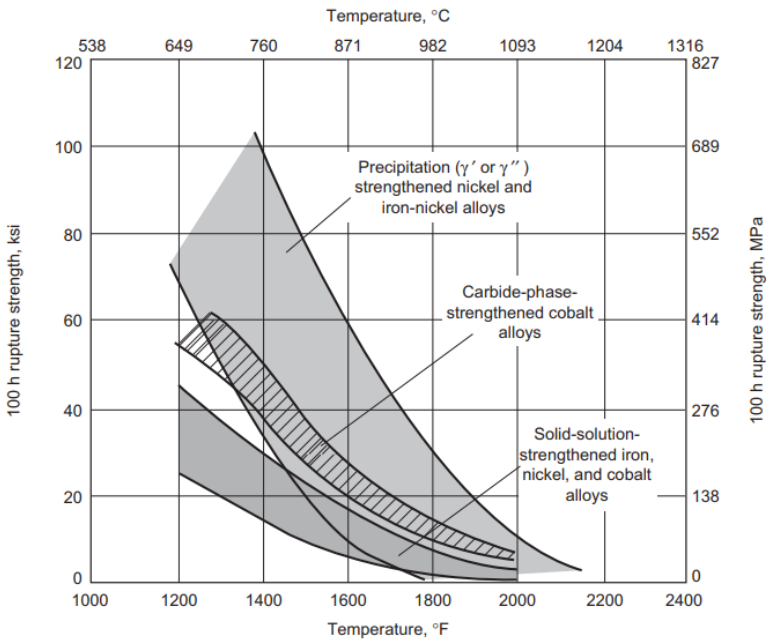

Figure 2.1 : Stress- rupture behavior of different superalloy groups [2].

2.1 Cobalt Based Superalloys

Cobalt-based superalloys are the second most popular alloy group used in the production of hot zone parts after nickel-based superalloys. Thanks to their higher melting temperature and better thermal stability than nickel, cobalt alloys have been a monopoly for many years, especially in the production of structural parts such as the stator, which immediately follows the combustion chamber in gas turbine engines [25,26]. The combustion chamber is a system where the compressed air coming from the compressor is burned with engine fuel and the expanding gas temperature reaches

2900 K [27]. The task of the stator is to direct these expanding hot gases to the turbine rotor at the right angle. Therefore, the stator material is expected to have sufficient thermal stability, creep resistance, strength and thermal fatigue resistance at high temperatures as well as high corrosion resistance [28]. Cobalt-based superalloys can meet these requirements. For this reason, stators in gas turbine engines have been manufactured from cobalt-based superalloys for many years [29].

Cobalt based alloys can be divided into 3 groups; high wear resistant alloys with high carbon content, low carbon containing alloys suitable for working under high temperature conditions and high corrosion and wear resistant alloys with low carbon content. The later group constitutes the majority of cobalt-based superalloys and is divided into two groups: wrought and cast alloys. Cast cobalt alloys contain approximately 50-60% cobalt with additions of 20-30% chromium, 5-10% tungsten and 0.1-1% carbon. In addition to the high carbon content, the addition of silicon is intended to increase the fluidity of the molten metal and ease casting. In wrought cobalt alloys, approximately 20% nickel is added separately from casting alloys and carbon addition is limited to 0.15%, thus increasing the ductility of the structure and improving its formability [26], [30]. The main strengthening mechanisms of cobalt-based superalloys are solid solution hardening and the interaction of carbide precipitates with dislocations. An example of carbide-dislocation interaction is shown in Figure 2.2.

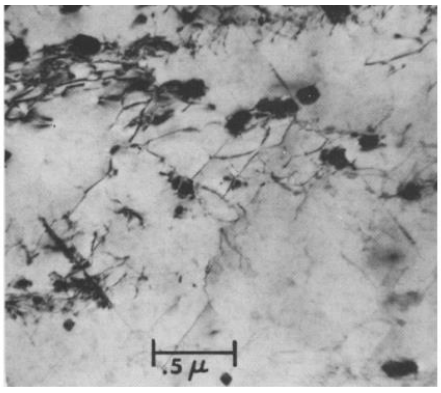

Figure 2.2 : Carbide and dislocation interaction of Haynes 188 alloy after creep test (927 °C/ 41.4 MPa) [31].

While zirconium, titanium, manganese, carbon alloying elements cause expansion in the matrix; chromium, molybdenum, tungsten and silicon elements cause contraction effect in the matrix. As indicated in Table 2.2; Chromium, molybdenum, tungsten, tantalum, niobium, titanium alloying elements are also carbide forming elements.

Chromium and aluminium increase oxidation and hot corrosion resistance by forming a protective oxide layer (Cr_2O_3 and Al_2O_3 respectively) on the material surface [31].

Table 2.2 : Effects of alloying elements on cobalt alloys' properties [31].

Element	Effect
Chromium	Oxidation and sulfidation resistance Carbide former
Molibdenum, Tungsten, Tanalum, Niobium	Solid solution hardening Carbide former Intermetallic phase (Co_3M)
Aluminium	Oxidation resistance Intermetallic phase (CoAl)
Titanium	Carbide former Intermetallic phase (Co_3Ti, Ni_3Ti)
Nickel	FCC stabilizer Intermetallic phase (Ni_3Ti)
Carbon	Carbide former

Cobalt-based superalloys increase their strength by dispersing the carbide precipitates they contain in the matrix and on grain boundaries, cobalt-based superalloys contain about 13% carbides. The formation and transformation of these carbides occur during solidification after casting and heat treatment. In cobalt-based superalloys, MC, M_6C, $M_{23}C_6$, M_7C_3, M_2C_3 carbides (M: Metal or metals, C: Carbon) can be found in coarse, block, chinese script, fine and spherical morphology, the carbides and their morphologies are affected by chemical composition and cooling rates. The most stable of these carbides are MC and M_6C carbides. So that, MC carbides can maintain their stability even at temperatures where the incipient melting is observed in the microstructure. Especially alloying elements such as tantalum, hafnium and zirkonium, which have high melting temperature and low solubility in cobalt, improve high temperature stability by forming MC carbides. M_6C is formed when the amount of tungsten and molybdenum in the alloy exceeds 5% [4,32,33]. The elements each carbide includes are listed in Table 2.3.

Table 2.3 : Carbide types and the elements they contain [34].

Carbide Type	Contained Elements
MC	Ti, Zr, W, Ta
M_7C_3	Cr
$M_{23}C_6$	Cr
M_6C	Mo, W

Cast cobalt alloys contain primary, coarse carbides such as; MC, M_7C_3 and $M_{23}C_6$. In the as cast microstructure, M_7C_3 and $M_{23}C_6$ carbides are eutectic and have a web morphology while the MC carbides are in block and chinese script morphology [32,35]. Oxidation mechanism of cobalt based superalloys is shown in Figure 2.3, typical oxidation mechanism takes place in the order of:

Firstly, grain boundary carbides and matrix react with oxygen to form $Co_4Nb_2O_9$ and then the matrix is oxidised to CoO and Cr_2O_3. At the same time, Cr_2O_3 is formed on Cr_6C at the grain boundaries. Product of CoO and Cr_2O_3, $CoCr_2O_4$ nodules appear, which grow until they cover the entire $Co_4Nb_2O_9$ formed on Cr_2O_3 and (W,Nb)C. The oxide layer consists of a single phase ($CoCr_2O_4$ spinel structure) and oxidation progresses on the substrate through grain boundary carbides. Oxidation of the grain boundary carbides releases CO gas, which creates a continuous path for oxygen penetration [14].

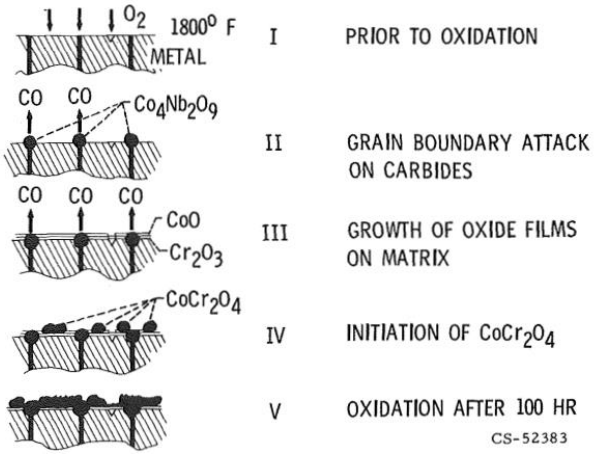

Figure 2.3 : Schematic figure of oxidation of WI-52 cobalt-based superalloy [14].

In the gas turbine engine applications, sulphur in engine fuel reacts with NaCl in the atmosphere to form Na_2SO_4. Hot corrosion is defined as the accumulation of Na_2SO_4 salt on the metal surface and the resulting sulphidation and can be divided into two types, Type I and Type II. Type I hot corrosion occurs at high temperatures and Type II hot corrosion occurs at relatively low temperatures. The alloying element that makes the greatest contribution to corrosion resistance in cobalt-based superalloys is chromium. In cobalt-based superalloys containing 30-40% Cr by weight, the formation of Cr_2O_8 or $CoCr_2O_4$ structures on the material surface prevents or retards the formation of eutectic Na_2SO_4-$COSO_4$ structure which has a low melting temperature [26], [31], [36].

2.2 Coatings For Superalloys and High Temperature Applications

For components used in the hot zones of gas turbine engines, corrosion is as critical damage mechanism as creep and low cycle fatigue damage. In order to avoid corrosion, chemical compositions of alloys are improved, but this alone is not sufficient so coatings such as thermal barrier coating, diffusion aluminide and overlay coatings (MCrAlY) are developed. These coatings provide oxidation and corrosion resistance to the material, while thermal barrier coatings also provide insulation up to 170 K, contributing to the increase of turbine inlet temperatures and thus engine efficiency [10,37].

Coatings used in high temperature applications can be divided into 3 main classes:

1. Thermal barrier coatings (TBC)
2. Overlay (MCrAlY) coatings
3. Diffusion coatings

The temperature enhancement and relative coating life of these methods can be seen in Figure 2.4.

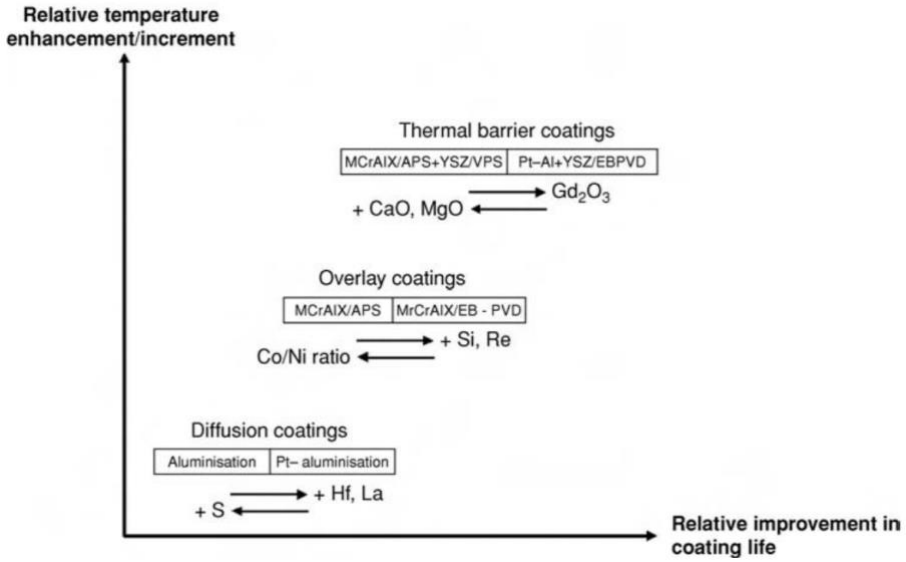

Figure 2.4 : High temperature coatings and their relative coating life and temperature enhancement [3].

Thermal barrier coatings basically consist of two layers. These are one ceramic exterior layer (top coat) and a bond layer which can be either an overlay (MCrAlY) or aluminide coating. Generally, the chemical composition of the most widely used ceramic layer is zirconium oxide (ZrO_2) with 6-8% yttrium oxide addition [38,39].

Unlike diffusion coatings, for overlay coatings, diffusion of the coating material into the substrate is not necessary. While some diffusion is essential for enhancing the adherence of the coating, overlay coatings don't depend entirely on diffusion for their development. The protection mechanism of overlay coatings (MCrAlY) is the protective oxide layer formation of the elements (Al, Cr, Y) in the coating composition. M stands for Ni or Co in some cases both [40].

Aluminum enables primary oxidation resistance by forming Al_2O_3, but chromium is proficient at mitigating hot corrosion and enhances the chemical reactivity of aluminum. A minimal quantity of yttrium enhances the adhesion of the oxidation product as it will prevent the formation of sulfur included harmful phases in the interphase of substrat and the coating [41].

2.2.1 Diffusion aluminide coatings

The application of diffusion aluminide coatings comprise of bringing an aluminium source into contact with the material at high temperature and diffusion-based reactions take place. The material surface reacts with aluminium to form the MAl (M: Metal) layer. For example, NiAl layer is formed in nickel-based superalloys and CoAl layer is formed in cobalt-based superalloys. At the same time, an interdiffusion layer between the MAl layer and the substrate material, is also formed. At high temperature MAl layer formed on the material reacts with oxigen and forms Al_2O_3 protective layer, which is stable even at temperatures above 900 °C and shows brittle behaviour below 750 °C [42,43].

Aluminide coating has been used for many years on hot zone parts in gas turbine engines. Aluminizing is applied by many processes that are used commercially, most common ones are; chemical vapor deposition (CVD), Pack aluminizing, above pack and slurry process as shown in Figure 2.5 [41].

Additives such as Pt and Cr can be added to aluminide coatings to increase the coating performance especially regarding hot corrosion. Aluminide coatings can be divided into 2 groups depending on the diffusion mechanism:

- High temperature low-activity aluminizing (outward diffusion)
- Low temperature high-activity aluminizing (inward diffusion)

In low-activity aluminizing, the rate of inward aluminum diffusion is slow compared to outward diffusion of nickel or cobalt, whichever is the main substrate metal. In low activity aluminizing, the coating forms mainly by Ni or Co diffusion resulting with the formation of NiAl or CoAl layer. In this type of aluminide coating, a diffusion heat treatent is applied after the coating prosess. In high-activity aluminizing, the main forming mechanism is aluminum diffusion into the substrate which is faster than nickel or cobalt diffusion. Rections of each method is shown in Figure 2.6 [44,45].

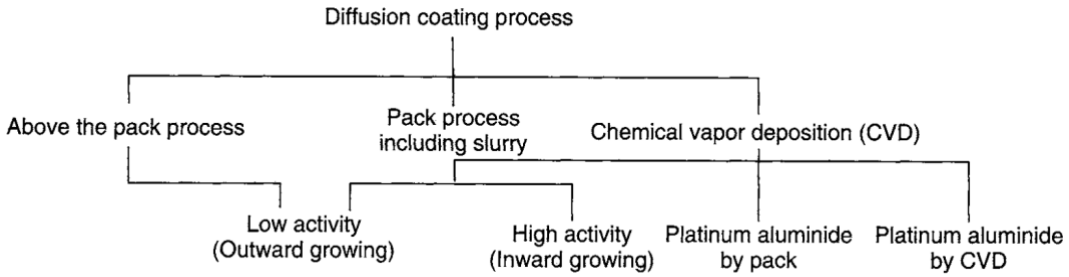

Figure 2.5 : Different diffusion coating methods [46].

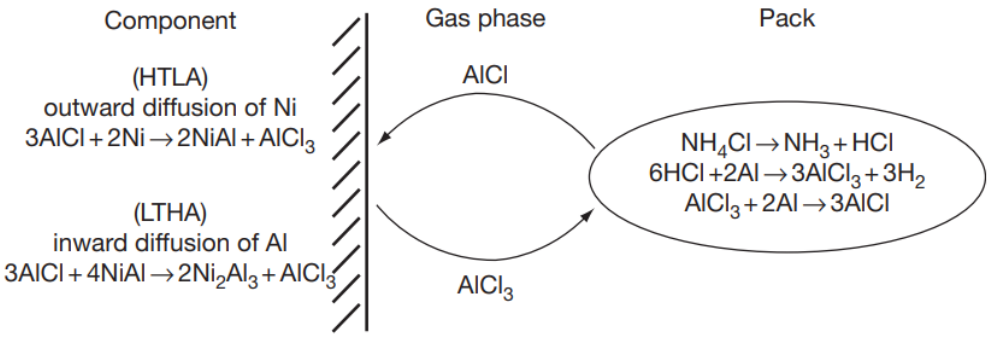

Figure 2.6 : Schematic image of chemistry in the pack aluminizing process [47].

2.2.1.1 Pack aluminizing process

Pack aluminizing is a process where the aluminum source, a halide activator (generally NaCl), and a stable powder (mainly alumina) are mixed together. This mixture is in powder form and the part to be coated is buried in this powder mixture in a container as shown in Figure 2.7. The container is then heated in a furnace in order to promote diffusion. The process generally takes place in a argon or hydrogen environment in order to prevent any oxidation at process temperatures. Alumina provides the porous structure that will allow gas transfer during the process, while at the same time, it preserves pack powder mixture from sintering caused by exposing to high temperatures for a long time. Pack composition examples can be seen in Table 2.4 [48,49].

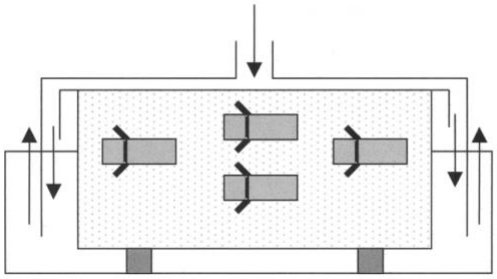

Figure 2.7 : Schematic image of the pack process [41].

At high temperatures, halide activator decomposes, and the halogen (Cl in the case of NaCl) reacts with aluminum source to produce aluminum halides (generally $AlCl_3$). The surface of the part is then reacts with $AlCl_3$ and as the diffusion proceeds, the coating forms [41]. The primary advantages of the pack technique are excellent coating repeatability and reduced cost. The drawbacks include restrictions on the compositional flexibility of the coating and limitations on its thickness. Additionally, in the MAl layer (for example CoAl or NiAl) some powder particles from coating mixture might be trapped. These particles cause discontinuous coating structure and lowers the coating life as well as it's protectiveness. The restricted range of coating thickness attained in this method results from two issues. Coating thickness that can be formed by pack aluminizing is effected by time as this process is run by diffusion and composition of pack [41]. Using slurry as a coating media is another way to perform pack aluminizing. In this method powder mixture includes a binder also. The mixture can be applied to the surface of the part by spraying, brushing, or dipping methods. After the mixture is applied to the part, a heat treatment is conducted to start diffusion . This is rather a simple method and it isn't efficient for complex geometries [50].

Table 2.4 : Examples of aluminide pack compositions [47].

Pack Constituent	LTHA pack	HTLA pack
Process temperature	700-900 °C	950-1000 °C
Aluminum flake	1.7-2.7 wt%	1.2-1.5 wt%
Activator		
NaF	0.8-1.2 wt%	0.8-1.2 wt%
KHF	0.05-0.15 wt%	0.05-0.15 wt%
NH_4Cl	0.1-0.2 wt%	0.1-0.2 wt%
AlF_3	Trace	Trace
Alumina	Balance	Balance
Uncombined water	<0.3 wt%	<0.3 wt%

2.2.1.2 Above pack process

During this procedure the pack in powder form is kept in a tray-like structure and parts that designated for coating are situated on the pack (Figure 2.8). The parts and the pack system are placed inside a furnace. The carrier gases fed into the furnace carry the halides produced in the pack at high temperature and enable the part to be coated. This process generally produces a low activity coating and offers a more uniform coating thickness than the pack aluminizing process. Diffusion coatings exhibit brittleness below a transition temperature, coating produced by the above pack method have lower temperature of transition than the coatings produced by pack aluminizing method, which may be associated with lower aluminum content [51,52]. The above-the-pack method also yields a pristine covering devoid of pack particle entrapment [47].

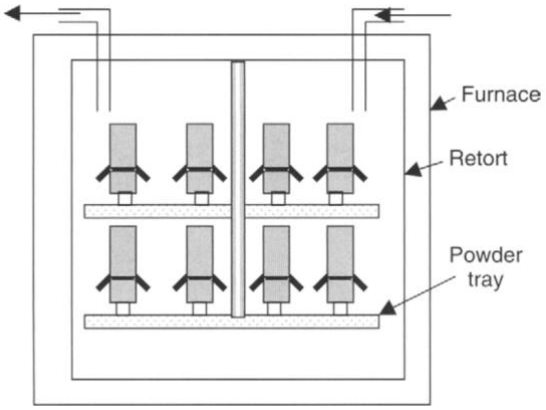

Figure 2.8 : Schematic image of above-pack process [41].

2.2.1.3 Chemical vapor deposition method

In the Chemical Vapour Deposition method, the Al source does not directly contact the part, halogen gases such as Cl_2 and HCl pass over the Al source (pellet, powder or chip) at approximately 300 °C, to form gases such as $AlCl_3$ and the parts are coated by contacting with this gas. H_2 and Ar are generally used as carrying gases [41]. A schematic image of the process is shown in Figure 2.9.

Process temperatures are generally between 1000-1100 °C. This method is the most widely used method in the industry today. This is because it is easier to control the process, is repeatable and has better adhesion compared to Pack aluminizing and slurry methods. In addition, it is much easier to carry out modified aluminide coating

experiments with the addition of different elements (Y, Hf, Zr, etc.) in the CVD method because these element sources can be easily integrated into the device [53].

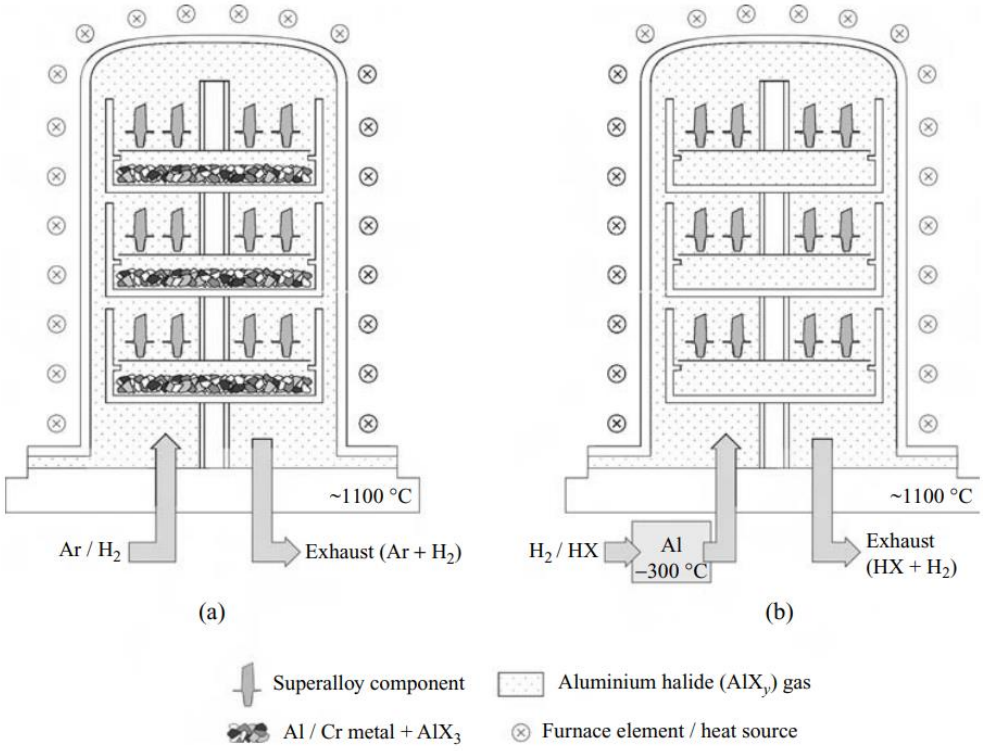

Figure 2.9 : Schematic diagram of a) above-pack process and b) CVD process where the aluminide halides generated externally [41].

If the CVD process is low activity then the Al source and halogen gases react in a diffrerent environment than the coating process chamber, if the process is high activity, this reactions takes place at the coating process chamber [41] .

3. EXPERIMENTAL DETAILS

In this study, homogenization and pack aluminizing coating processes were applied to a cobalt alloy in as-cast condition and the effects of these processes on microstructure changes and room temperature tensile and stress-rupture behaviour were investigated.

3.1 Material

A cobalt-based cast superalloy, whose chemical composition is shown in Table 3.1 was used in the study. The chenical analysis was conducted with Hitachi OES750 The alloy has high oxidation and corrosion resistance due to its high Cr content. In addition, the W, Nb, Mo elements it contains combine with C to form carbides, which is the main strengthening mechanism.

Table 3.1 : Chemical composition of the cobalt-based superalloy (wt.%).

Element	Cr	W	Nb	Mo	Fe	Ni	C	Si	Mn	Ta	Co
Composition (wt. %)	22.4	10.1	1.5	0.2	1.8	1.6	0.4	0.4	0.1	0.04	Balance

3.2 Heat Treatment Procedures

Homogenization process was applied to the cast condition samples at different temperatures and times. ThermoCalc software was used to determine the homogenization temperature. The homogenization process conditions applied are shown in the Table 3.2.

Table 3.2 : Homogenization conditions applied.

Designation	Temperature (°C)	Time (h)
HT1200-1	1200	1
HT1250-1	1250	1
HT1250-10	1250	10

All heat treatments were carried out in a Protherm PLF 130/30 muffle furnace. The hardness and carbide volume fractions of the as-cast and heat treated samples were measured (the details was given in the next section), and the chemical compositions of the phases in the microstructure were analysed and compared.

3.3 Pack Aluminizing Procedure

Pack aluminizing process was applied to the as cast and homogenised HT1250-10 samples at 1040 °C for 4 hours and then cooling in the furnace.

As a solution to the inhomogeneous coating, pack aluminizing was applied to samples with different surface conditions (cut surface, polished surface and 400 grit blasted surface) under the same conditions. Pack aluminizing conditions were determined in the light of the data obtained from the literature [15]. The powder mixture used was consist of 70% Al_2O_3, 25% Al and 5% $AlCl_3$.

3.4 Microstructural Characterization

Microstructural analysis was performed by using samples with dimensions of 10 x10 x5 mm^3. The samples were cut with a QATM precision cutting device. Bakelite samples were sanded from 320 mesh to 2500 mesh and then polished with 3 µm and 1 µm polycrystalline diamond suspension. The microstructure emerged after these processes, no extra chemical etching was applied. This is due to the high hardness difference between the carbide structures and the matrix. The microstructure of the prepared samples was observed with Nikon optical microscope and Hitachi SU5000 scanning electron microscope (SEM), Oxford Ultim 40 mm^2 EDS detector was used to observe chemical composition of the each phase in the coating and substrate microstructure. Carbide volume fraction calculations were performed using ImageJ image processing software on the SEM images taken from 10 different regions of each sample. XRD analysis is made after coating process, in order to determine the aluminide layer structure. The analysis was performed with GBC MMA 027 model device using CoKα radiation. The scanning of the samples was performed with 0.02° steps in the range of 10°- 90°.

3.5 Mechanical Characterization

3.5.1 Hardness test

Hardness tests was carried out by using a Rockwell C hardness tester (QATM Qness 250 EVO) at a test load of 150 kgf on 5 areas of each sample to obtain the average hardness value. To determine the hardness of each coating layer after pack aluminizing, nanoindentation hardness measurement is applied. The nanoindentation method (CSM nanoindentation tester, Berkowich indenter) was used to measure the hardness of each layer formed after aluminide coating.

4. RESULTS AND DISCUSSIONS

Under this heading, the results of microstructure examinations, hardness, tensile test and stress-rupture test results of the cast cobalt superalloy after casting condition, homogenization process and pack cementetion aluminide coating conditions are described and comparisons are made.

4.1 Process Design of Homogenization

Homogenization temperature was determined by using ThermoCalc software. Figure 4.1 shows temperature dependent change of volume fraction of phases. Homogenization temperature should be above the dissolution temperatures of all phases, as seen from the volume fraction curves, some of the phases (MC) exist in the microstructure even above the incipient melting temperatures. According to ThermoCalc calculation incipient melting temperature is 1269 °C.

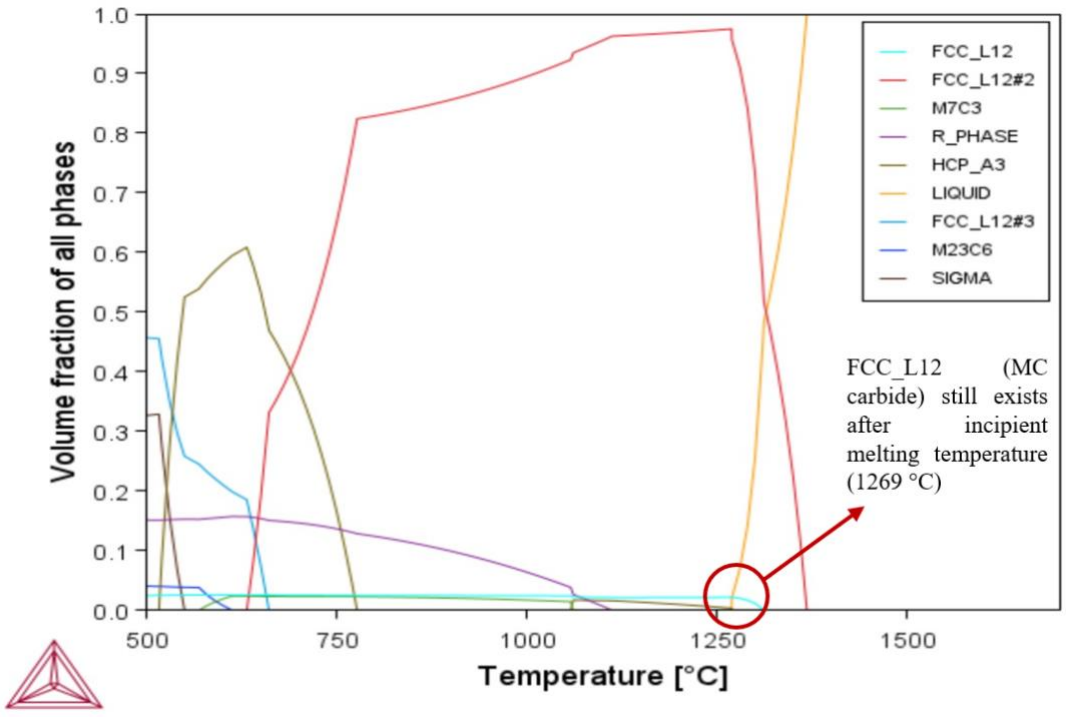

Figure 4.1 : Temperature dependent change of volume fraction of phases for the alloy used in this study.

4.2 Microstructural Characterization

4.2.1 Microstructure of received material

As seen from Figure 4.2, the microstructure of the casting contained matrix, two types of carbide and SiO_2 inclusions with net-like and Chinese script morphologies. Carbides were homogeneously distributed throughout the microstructure and the presence of SiO_2 indicates that the casting took place under air atmosphere. The carbide volume fraction in the microstructure was 6% and the as-cast dentritic structure was evident. EDS analysis (Figure 4.3) showed that the net-like carbide was rich in Cr and W, while the carbide with Chinese script morphology was rich in Nb. As it is indicated in several literature the Nb rich carbide is MC type and Cr-W rich carbide is $M_{23}C_6$ type [32], [35].

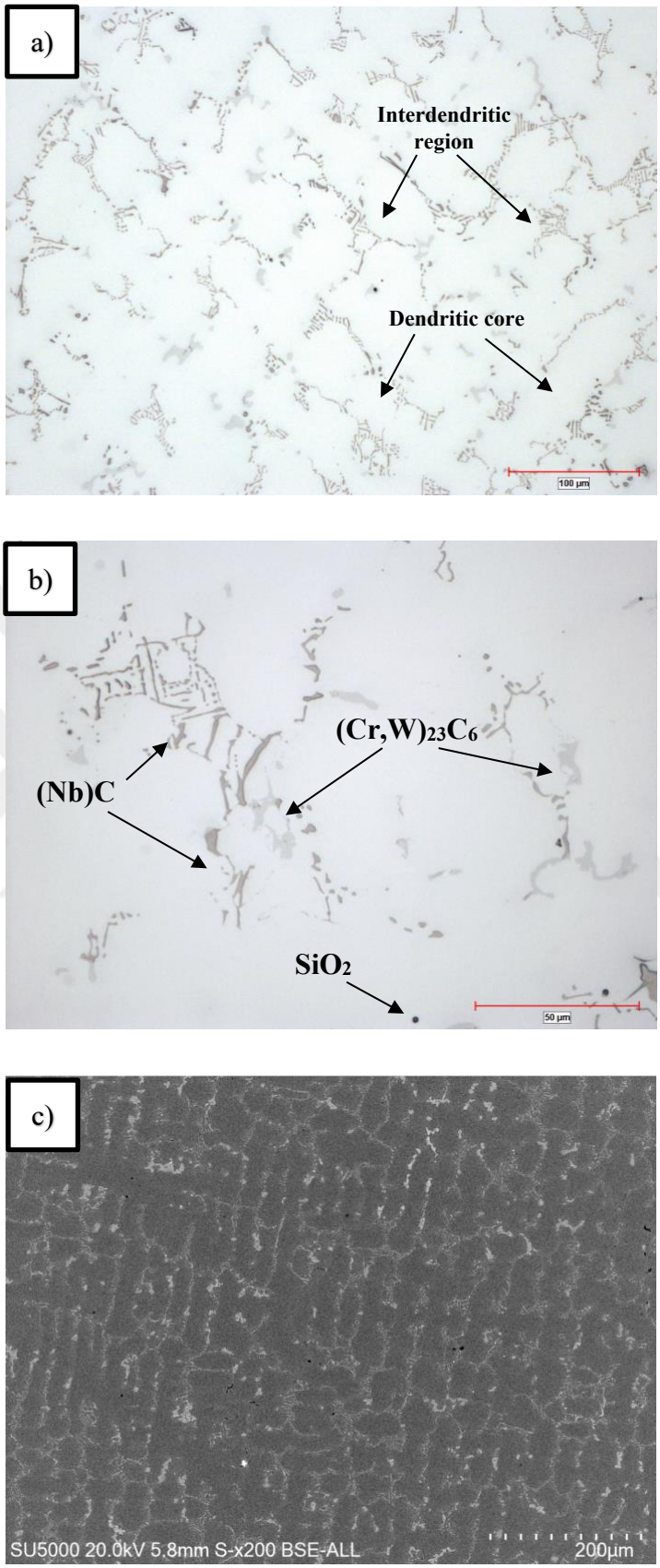

Figure 4.2 : Optical micrographs in different magnifications (a,b) and SEM (c) micrograph of the as received sample (as-polished).

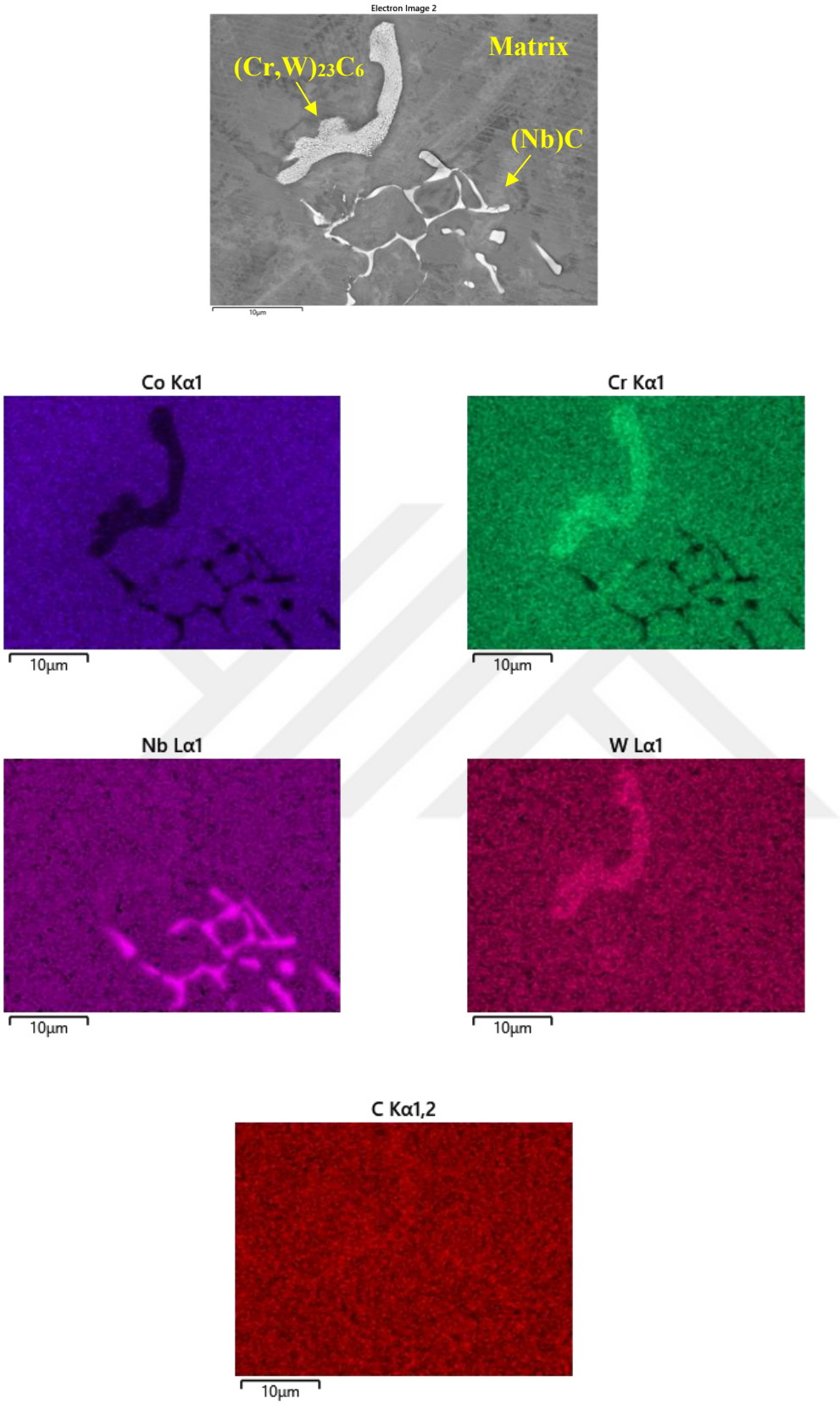

Figure 4.3 : EDS mapping analysis of as received sample.

4.2.2 Post homogenization microstructure

As a result of the homogenization attempt at 1200 °C for 1 hour, it was observed that there were not any significant changes in carbide morphology and volume fraction. Dendrite structure was not affected by the homogenization treatment.

After holding the as recieved sample at 1250 °C for 1 hour, it was observed that approximately half of the carbides were dissolved. Although, the dendrite structure was not changed significantly, morphologies of the carbides were changed from continuous to discontinuous. It was decided to increase time instead of temperature due to the risk of melting.

After 10 hours at 1250 °C, it was observed that the amount of carbides decreased slightly more, but the rate of change slowed down. The $(Cr,W)_{23}C_6$ carbides were dissolved to matrix and the morphology of the NbC carbides were changed from chinese script to spherical, thin and discontinuous morphology that spreaded more homogeneous around the matrix. Dendrite structure was also disrupted. As can be seen from the ThermoCalc calculations, the presence of some carbide after homogenization heat treatment is acceptable because some of the phases are present even after beginning of the melting. Since further increase in temperature may cause melting, the rate of carbide and hardness decrease gradually decreases and the equipment is not suitable for increasing the time, 1250 °C for 10 hours was accepted as the optimized homogenization condition.

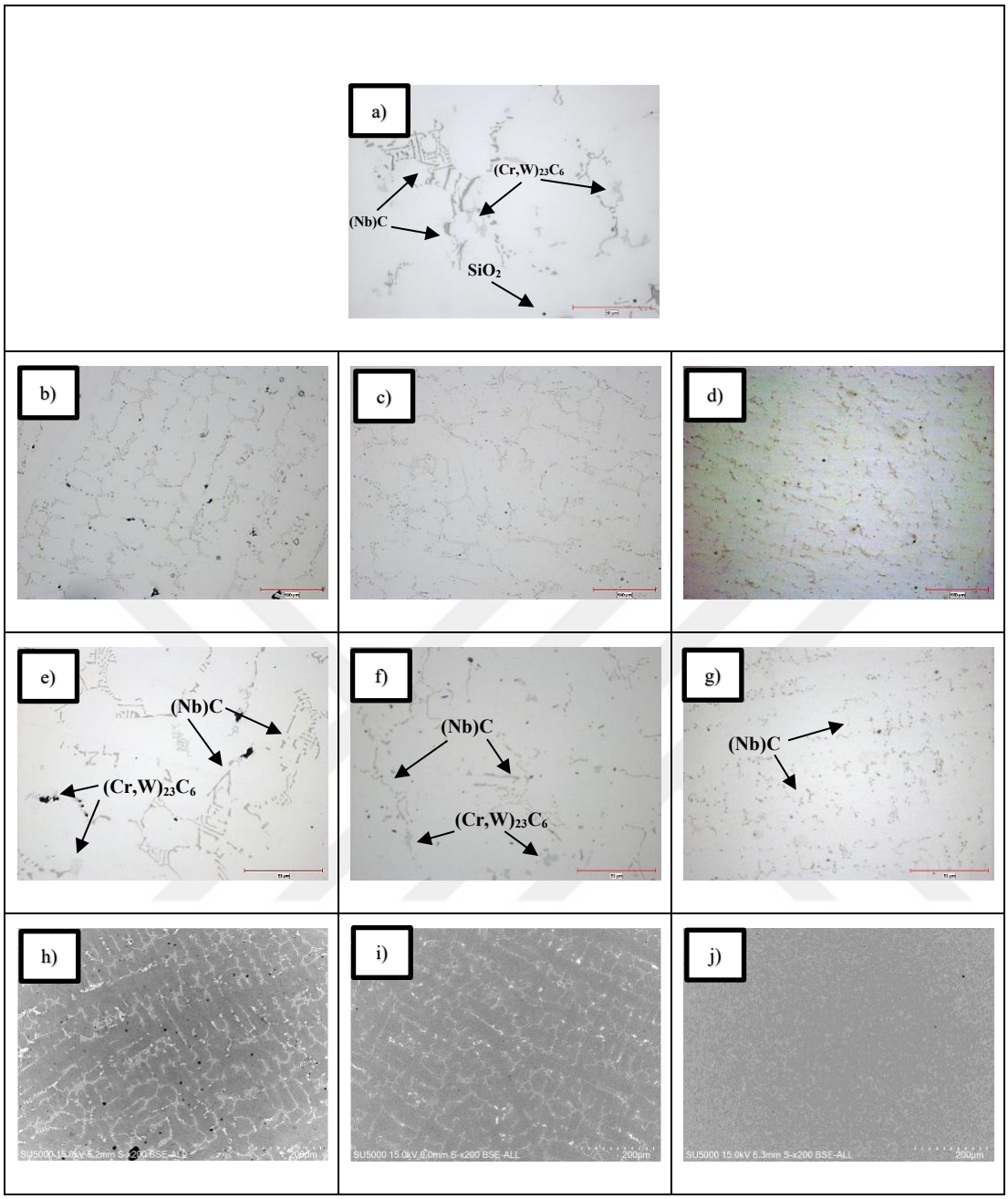

Figure 4.4 : Optical micrograph of as received sample (a), optical micrographs and SEM images of HT-1200-1 (b,e,h), HT-1250-1 (c,f,i) and HT-1250-10 (d,g,j) samples.

4.2.3 Carbide volume fraction and hardness calculations

After 1 hour at 1200 °C, the carbide volume fraction did not decrease significantly. ThermoCalc calculations showed that many phases existed at this temperature, so this was an expected result. The result of ThermoCalc calculation shows that after homogenization at 1250 °C, only the MC phase will be seen in the microstructure. The heat treatment results also confirmed this calculation as the main decrease in the carbide volume fraction was observed after homogenization at 1250 °C. This graph

shows the relationship between hardness and carbide volume fraction. These two values are directly proportional.

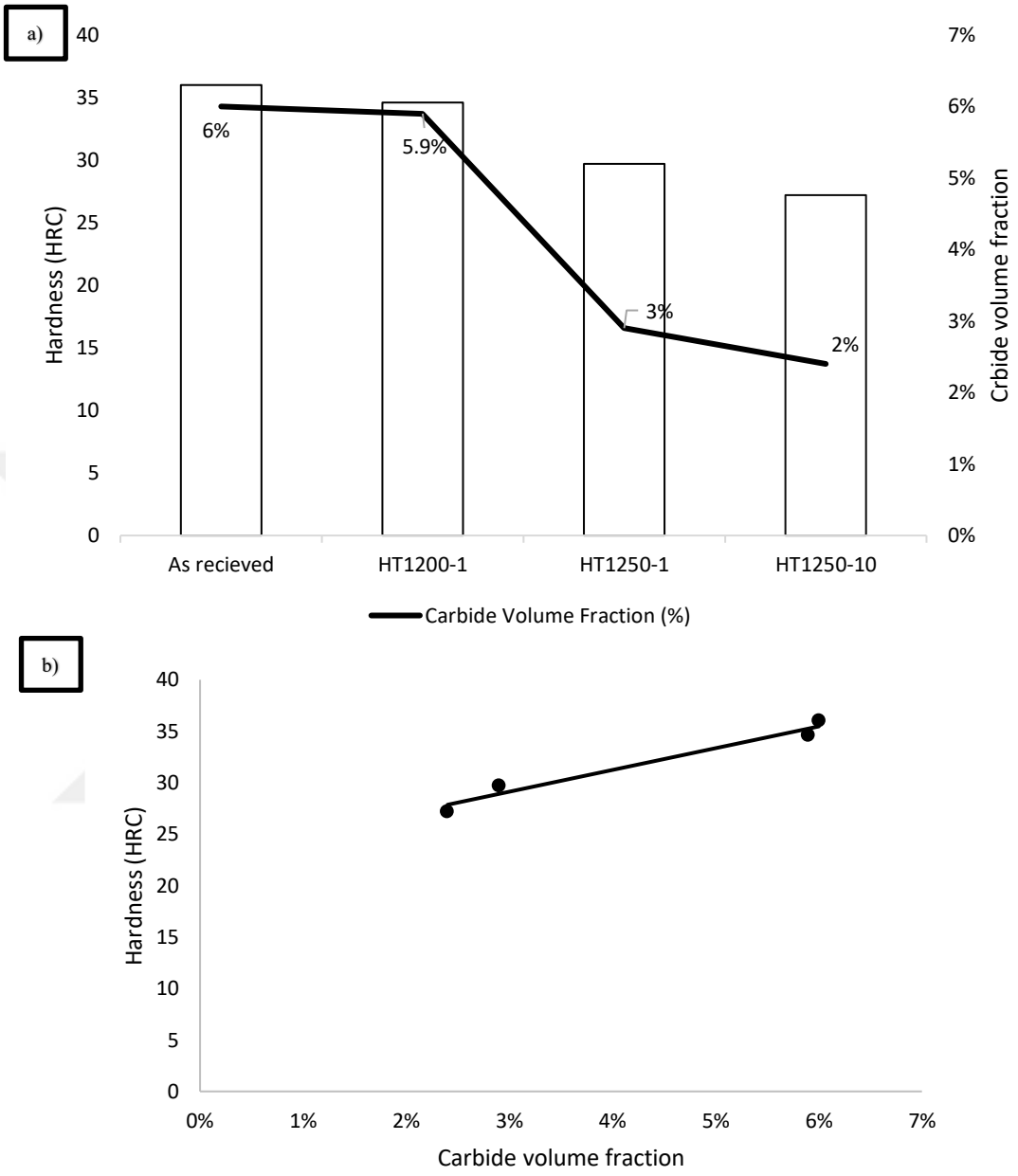

Figure 4.5 : (a) Carbide volume fraction and hardness change of different conditions, (b) Hardness and carbide volume fraction dependency.

4.2.4 Post pack aluminizing microstructure

The coating microstructure consists of 4 different layers with a total thickness of 280 µm. In previous studies, coatings with a thickness of approximately 50-60 microns were obtained using packs of different chemical compositions. The difference between the coating thicknesses is thought to be due to the pack composition. In this study, 70% Al_2O_3, 25% Al and 5% Al_3Cl pack compositions and different surface preparations

(120 grit grinding, 400 grit grinding, post-cut surface and polished surface) were used for pack aluminizing.

These layers are named as outer and mid coating layer, inner (interdiffusion) layer and thin layer from the outside to the center, respectively. The top layer of the coating has horizontal, continuous cracks. These cracks indicate the fragility of the top layer. In the outer coating layer, the matrix consists of light and dark gray spots with coarse carbide and black, coarse Al_2O_3 structures with elongated morphology, this layer is 240 µm thick and constitutes about 85% of the coating thickness. This outer layer consists of two distinguished layers, the outer one has a coating strusture of columnar morphology.

Below this layer, unlike the unprecipitated outer coating layer, there is a mid precipitated coating layer where fine carbide structures are precipitated and Al_2O_3 structures are not observed. It was observed that the fine carbide structures end in the precipitated mid coating layer from the substrate to the outer surface, but the coarse carbides continue. The thickness of this layer is approximately 21 µm and has the same thickness as the interdiffusion layer below it. Coarse and fine carbides are also present in the interdiffusion layer. As shown in Table 4.2, the coarse carbides are MC, rich in Nb and W, while the fine carbides are $M_{23}C_6$ rich in W and Cr.

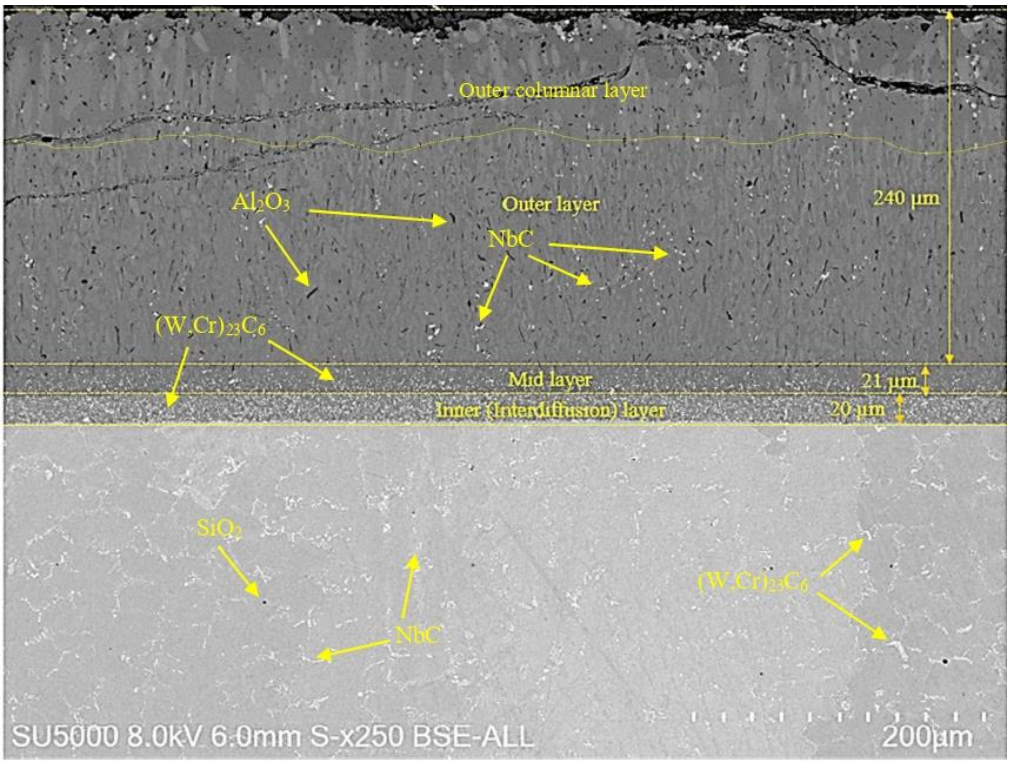

Figure 4.6 : Coating microstructure of as-cast sample

Point EDS analyzes were taken from the matrix of each coating layer. As a result of these analyzes, it was observed that the Al and Co ratios in the outermost layer were close to the Co_4Al_{13} chemical composition. As expected, the amount of cobalt decreased and the amount of aluminum increased from the substrate to the coating surface. It is seen that the amount of W decreases outwards. This decrease indicates that the diffusion of W, which is a heavy and refractory metal, is not fully achieved at the coating temperature and time. Cr content did not show a linear increase or decrease. Particularly high Cr and relatively high W content was observed in the thin layer formed between the substrate and inner layer, formation of a thin Cr-W rich layer has been observed before [13]. It is likely that this formation is because Cr and W also diffuse into the Co-Al layer formed during the coating process, but slower than Co. EDS results and the atomic % correspondence are given in Table 4.1 and Figure 4.7.

Table 4.1 : At. % Co and Al composition of each layer and substrate.

	Co	Al	W	Cr
Outer layer dark matrix	23.43	73.37	0.23	2.97
Outer layer light matrix	14.23	76.34	1.47	7.93
Mid layer	20.84	73.79	0.32	5.07
Interdiffusion	45.53	53.29	0.28	0.88
Thin layer	47.65	3.14	4.65	44.56
Substrate	72	-	3.65	24.35

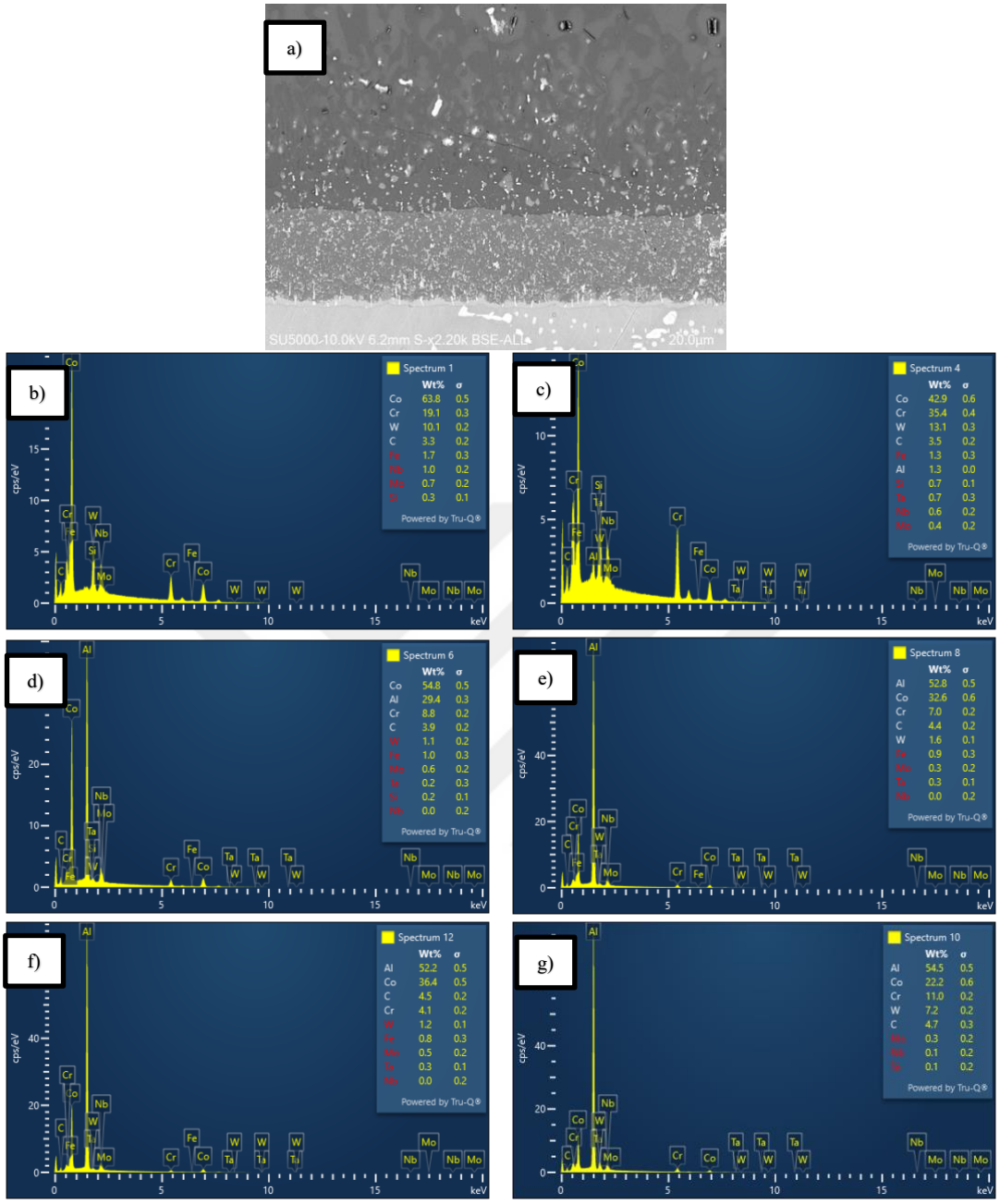

Figure 4.7 : Matrix composition of substrate (b) and each coating layer, thin layer (c), interdiffusion layer (d), mid layer (e), outer layer dark gray (f) and outer layer light gray (g).

Between the substrate and the interdiffusion layer there is a thin, well adherent and distinguishable layer with a saw-toothed morphology. The thickness of this layer is about 2 µm thick. This thin layer is shown in Figure 4.8.

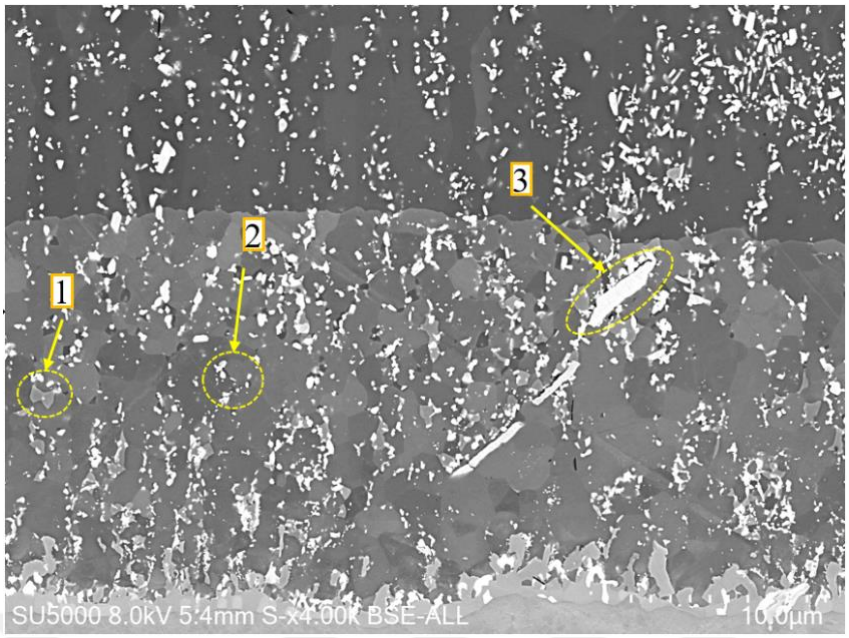

Figure 4.8 : Coating micrographs of as-cast sample in different magnifications.

Point EDS analysis was performed to find the phases of the precipitates observed in the coating layer. As a result of the analysis, it was seen that the fine carbides in the inner and mid layer were $(W,Cr)_{23}C_6$ and the coarse blocky carbides were NbC. The gray phase is thought to be Cr-Al intermetallic. EDS results and their atomic% correspondence are given in Table 4.2 and Figure 4.9.

Table 4.2 : Chemical composition (at.%) of structures indicated in Figure 4.9.

	C	W	Nb	Cr	Co	Al
1 (Gray precipitate)	13.53	4.48	-	23.37	2.69	55.93
2 (Cr, $W_{23}C_6$)	50.63	27.16	-	22.22	-	-
3 (NbC)	65.56	1.49	32.95	-	-	-

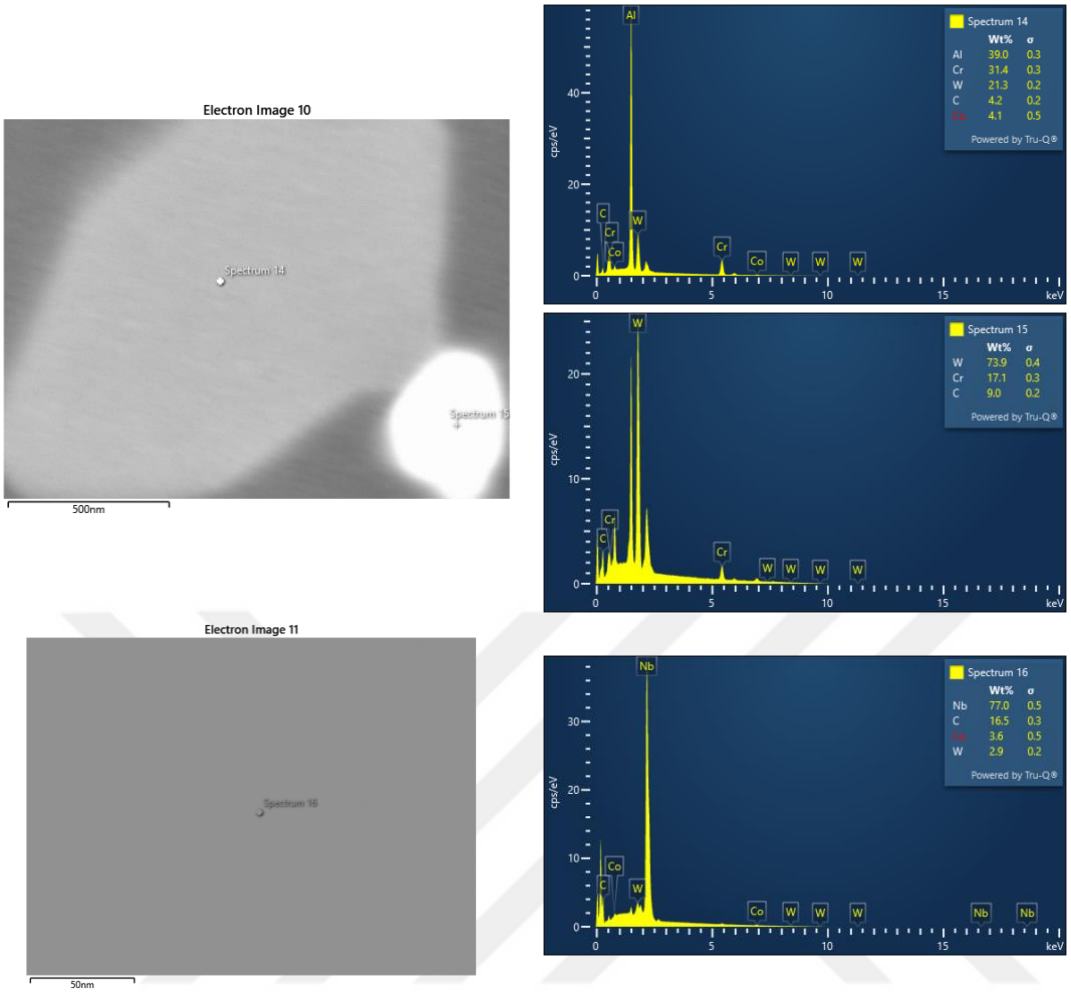

Figure 4.9 : EDS analysis of precipitates found in coating microstrusture.

EDS mapping clearly shows that the amount of Al decreases from the outer to the inner layers of the coating and is absent in the substrate. The amount of Co decreases from the center outwards but is present even in the top layer. This is also shown in Figure 4.11 as EDS line analysis of 100 µm line from the outer layer of the coating to the substrate. The Co content is higher in the closed gray areas in the matrix of the unprecipitated coating layer than in the light gray areas. In the thin layer, interdiffusion layer and a part of the top layer, W and Cr rich $M_{23}C_6$ carbides are observed. The Nb-rich coarse MC carbides in the substrate remained present throughout all layers of the coating.

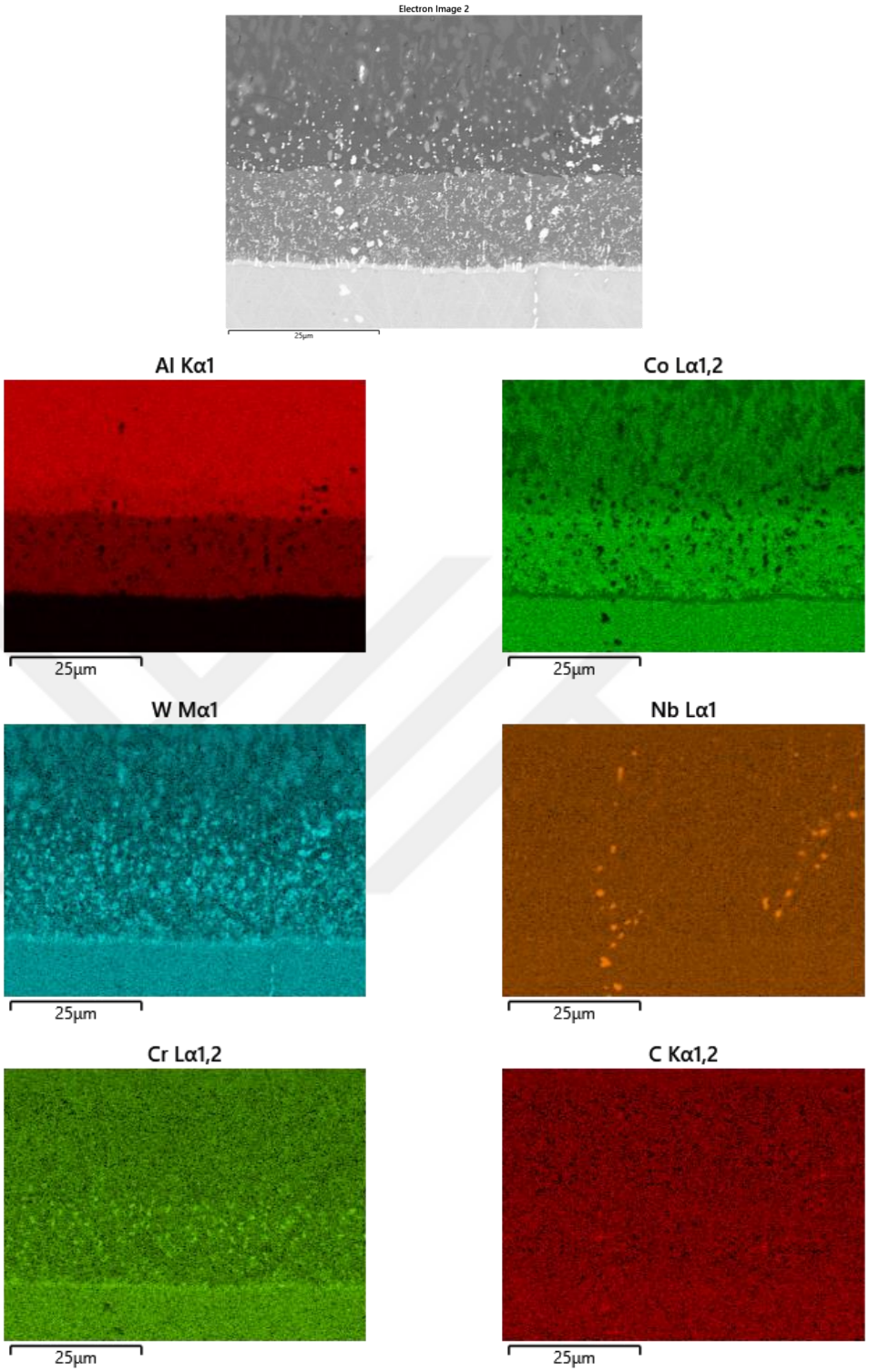

Figure 4.10 : EDS mapping of coating microstructure.

Line EDS shows that aluminum decreases towards the substrate and drops sharply to zero from the end of the interdiffusion layer. Considering that there is no aluminum in the substrate, this analysis indicates that the diffusion of aluminum into the substrate is dominant in used coating conditions. On the other hand, the amount of cobalt showed a more balanced decrease from the substrate outwards. The sudden drop at 75

microns and the subsequent increase is thought to be due to the possible presence of a precipitate.

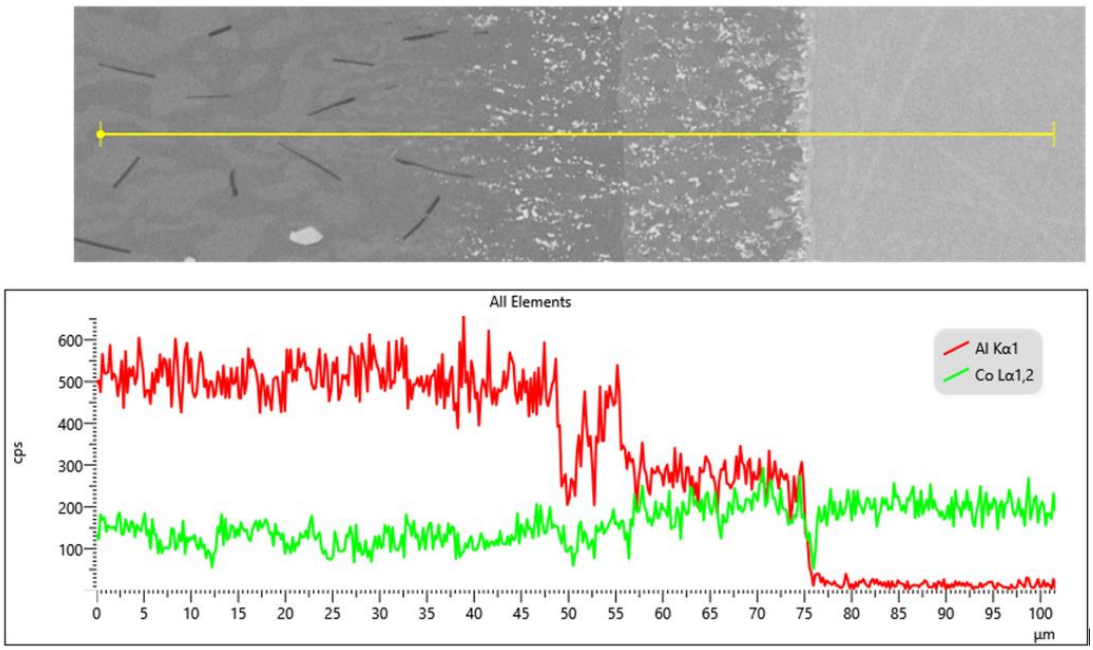

Figure 4.11 : EDS line analysis of coating microstructure.

XRD analysis was performed to determine the coating phase formed. The analysis results show that the outer layer is $Al_{13}Co_4$. The XRD result shows parallelism with the point EDS analysis taken from the outer layer matrix.

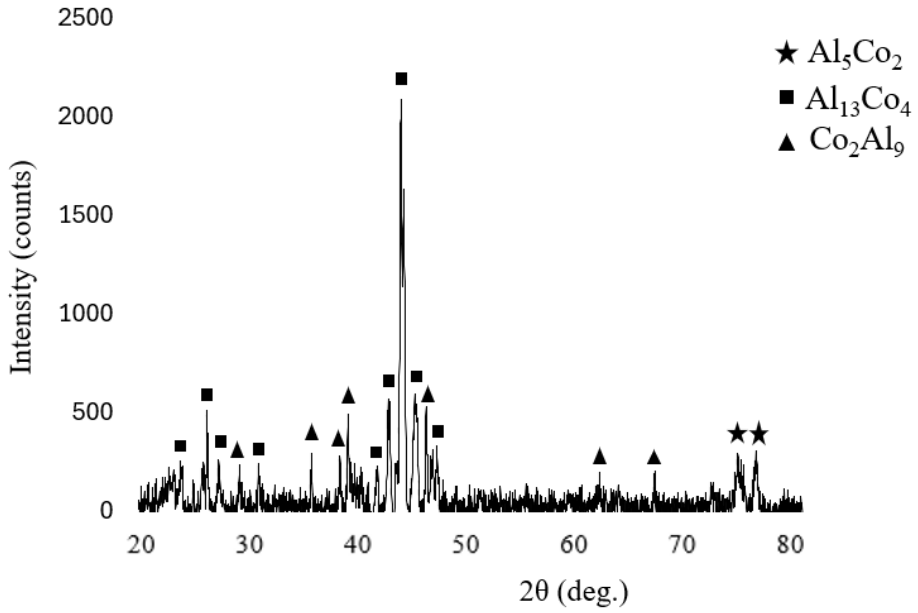

Figure 4.12 : XRD analysis of coated specimen.

As shown in Figure 4.13, the coarse carbide structure on the substrate continues throughout the coating. This is an indication of the inward diffusion of aluminum, in other words high activity aluminizing. Also it was observed that $(Cr, W)_{23}C_6$ carbides with a network morphology in the base material dissolved during coating process and re-precipitated as fine and homogeneously dispersed $(Cr, W)_{23}C_6$ carbides in the coating layer.

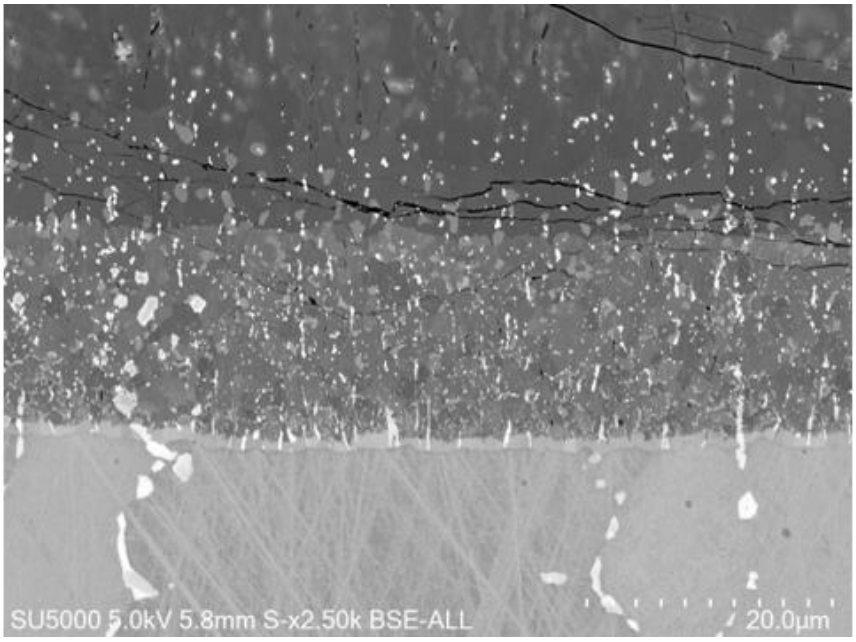

Figure 4.13 : Microstructure of the coated sample.

4.2.5 As cast and homogenized sample's microstructure after aluminizing

Samples in both as-cast and homogenization conditions showed the same coating microstructure and similar layer thicknesses. In both conditions, the coating thickness was up to 280 µm but wasn't consistent. The coating distribution including each layer was not homogeneous and there were many porosity and horizontal cracks, some of which were crater-like. $(Cr,W)_{23}C_6$ carbides were found in the inner and mid layers of the samples in both conditions. The fact that these carbides were removed in the structure after homogenization indicates that these precipitates were formed during coating.

The microstructures of both conditions are given in Figure 4.14.

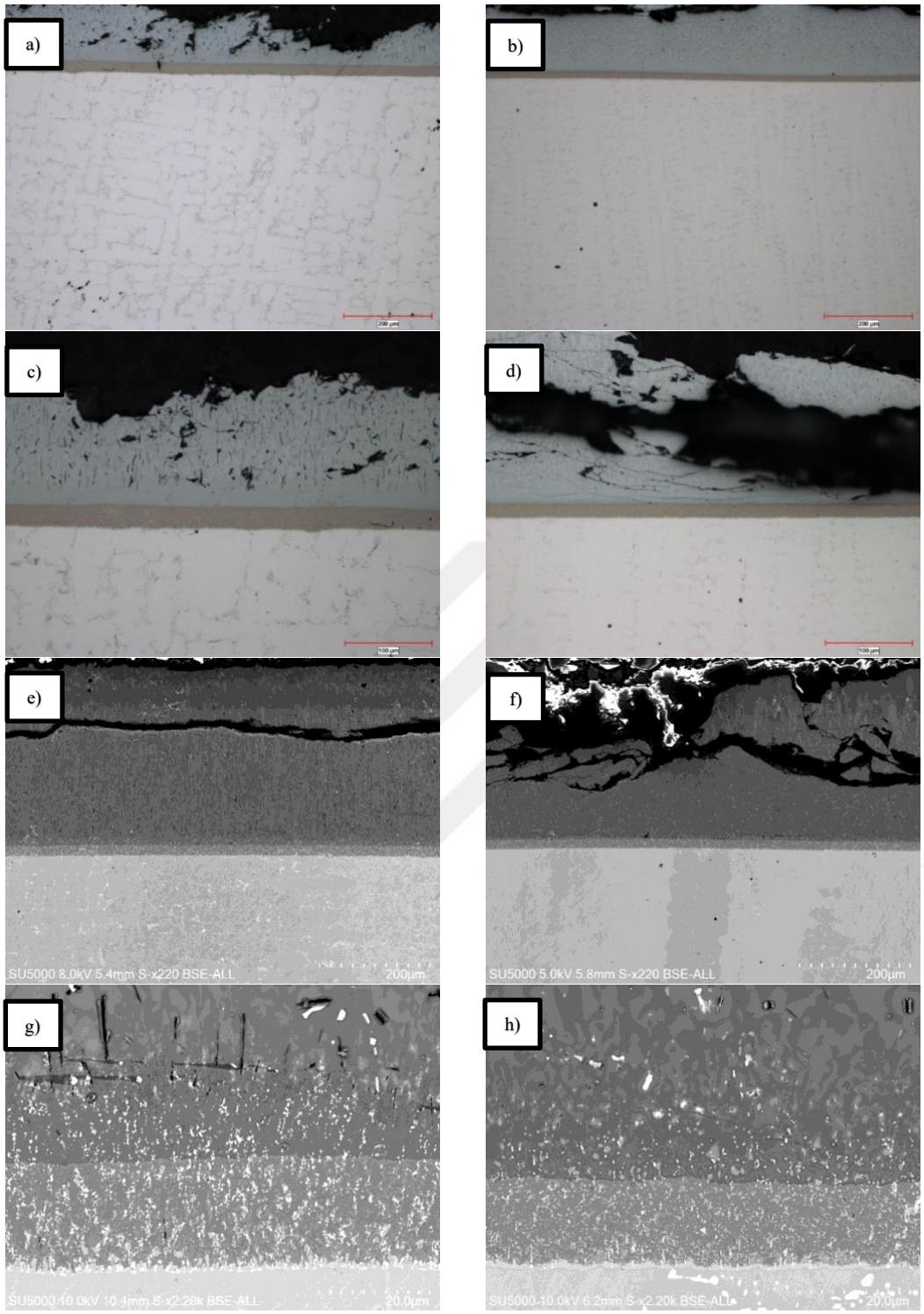

Figure 4.14 : (a-c-e-g) Microstructures of as-cast+ aluminide coated and (b-d-f-h) Microstructures of homogenized+ aluminide coated samples.

4.2.6 Microstructures of aluminizing after different surface preparations

Initial coating experiments showed that the coating thickness distribution was not homogeneous. To make the coaing thickness more uniform, different surfaces were prepared and coating experiments continued. Coating was applied to the surface after

precision cutting, after 400 grit grinding, after polishing and after 120 grit grinding. It was observed that the worst coating distribution was seen after 400 grit grinding. The polished surface, precision cutting surface and 120 grit grinding surface showed the most favorable results, respectively.

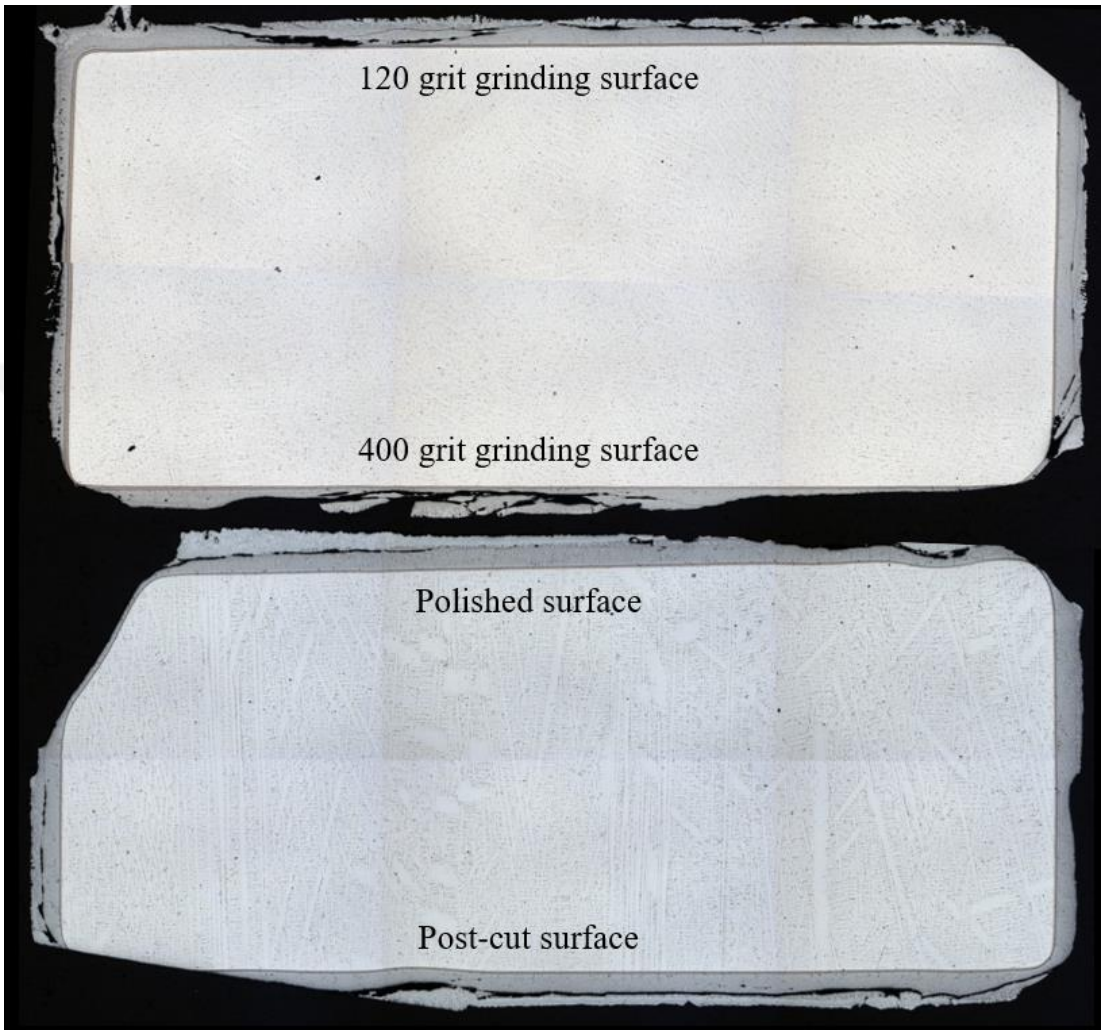

Figure 4.15 : Coating thickness distributon after different surface preparation conditions.

4.3 Coating Hardness Test

After the coating process, the hardness, elastic modulus, stiffness and elastic recovery values of each coating layer were measured using nanoindentation method. The results are given in Table 4.3. The substrate exhibits the lowest hardness, as expected for a relatively ductile cobalt-based superalloy matrix in its uncoated state. A substantial increase in hardness is observed in the inner (interdiffusion) layer. This suggests efficient inward diffusion of aluminum during the coating process and a dense,

homogeneous microstructure. The mid layer shows the highest hardness among all regions, likely due to the presence of highly ordered intermetallic compounds and possible residual stresses. While still significantly harder than the substrate, the outer layer exhibits a slight reduction in hardness compared to the mid and inner layers. This may be attributed to microstructural coarsening. The columnar region also displays elevated hardness, similar to the outer layer and slightly reduced hardness compared to the inner core of the coating.

The inner layer exhibits the highest elastic modulus. In contrast, the outer columnar layer shows the lowest modulus, potentially due to columnar grain morphology or porosity near the surface.

Stiffness follows a decreasing trend from the substrate to the outer layers, reflecting reduced substrate support and increased surface compliance in the coated regions.

Elastic recovery, which indicates the material's ability to return to its original shape after deformation, is significantly improved in all coated layers compared to the substrate. The mid layer shows the highest recovery, followed closely by the outer regions, suggesting that these layers possess a favorable balance of elasticity and hardness, enhancing damage tolerance under cyclic loading.

Table 4.3 : Hardness and elastic behavior of each coating layer.

Region	Hardness (GPa)	E (GPa)	Stiffness (mN/nm)	Elastic Recovery (%)
Substrate	4.5 ± 0.2	223 ± 14	1.8 ± 0.1	8.8 ± 0.5
Inner layer	11.5 ± 0.5	288 ± 13	1.5 ± 0.2	16 ± 1.7
Mid layer	12.4 ± 0.6	243 ± 20	1.1	20.5 ± 0.4
Outer layer	9.5 ± 0.4	198 ± 10	1.1 ± 0.1	19 ± 1.2
Outer columnar layer	9.4 ± 0.2	185 ± 4	1	19.7 ± 0.6

5. CONCLUSIONS AND RECOMMENDATIONS

The following conclusisons can be drawn from the present thesis study.

- It was observed that as the homogenization times and temperatures increased, the carbide morphologies changed from the initial continuous and Chinese script morphology to discontinuous, thin and spherical morphology.
- The carbide volume fraction and the hardness of the material decreased as the homogenization times and temperatures increased.
- There was no significant change in the chemical composition of the carbide phases.
- It was determined that the dentritic structure existing after casting was eliminated especially after homogenization at 1250 °C for 10 hours.
- After alumizing is applied to the as cast and homogenized samples, coating thicknesses of up to 280 μm were achieved, but a homogeneous coating thickness could not be obtained.
- According to the EDS and XRD analysis the outer layer of the coating is Al13Co4.
- After the aluminizing coating, a thin layer was formed on the substrate followed by an interdiffusion layer and then precipitated and unprecipitated coating layers respectively. Thin and homogeneously dispersed Cr, W23C6 inclusions showed continuity from the thin layer to the unprecipitated layer boundary. Coarse NbC carbides showed continuity in the substrate throughout all coating layers.
- Of the coating layers, the mid and inner layers were found have the highest hardness and elastic modulus. Stiffness values decreased from the substrate to the surface.
- In order to obtain homogeneous coating thickness, different surface treatments were tried before coating and the surface after polishing gave the best results.

REFERENCES

[1] **S. Biswas, S. Ramachandra, P. Hans, and S. P. S. Kumar,** "Materials for Gas Turbine Engines: Present Status, Future Trends and Indigenous Efforts," *J Indian Inst Sci*, vol. 102, no. 1, pp. 297–309, Jan. 2022, doi: 10.1007/S41745-022-00295-Z/FIGURES/7.

[2] **J. R. . Davis,** *ASM specialty handbook : nickel, cobalt, and their alloys*. ASM International, 2000.

[3] **R. C. Reed,** "The Superalloys: Fundamentals and Applications," *The Superalloys: Fundamentals and Applications*, vol. 9780521859042, pp. 1–372, Jan. 2006, doi: 10.1017/CBO9780511541285.

[4] **S. A. Sani, H. Arabi, S. Kheirandish, and G. Ebrahimi,** "Investigation on the homogenization treatment and element segregation on the microstructure of a γ/γ′-cobalt-based superalloy," *International Journal of Minerals, Metallurgy and Materials*, vol. 26, no. 2, pp. 222–233, Feb. 2019, doi: 10.1007/s12613-019-1727-7.

[5] **MORRAL FR,** "Corrosion of Cobalt and Cobalt Alloys," *Corrosion*, vol. 25, no. 7, pp. 307–322, Jul. 1969, doi: 10.5006/0010-9312-25.7.307.

[6] **A. Sezavar and S. A. Sajjadi,** "A review on the performance and lifetime improvement of thermal barrier coatings," *J Eur Ceram Soc*, vol. 45, no. 8, p. 117274, Jul. 2025, doi: 10.1016/J.JEURCERAMSOC.2025.117274.

[7] **M. Chen, K. Feng, M. Li, and C. Zhou,** "Hot corrosion behaviour of Al-Si-Dy coating on new γ′-strengthened cobalt-based alloy," *Corros Sci*, vol. 166, Apr. 2020, doi: 10.1016/J.CORSCI.2020.108431.

[8] **Y. J. Tang, Q. M. Wang, F. H. Yuan, J. Gong, and C. Sun,** "High-temperature oxidation behavior of arc ion plated NiCoCrAlYSiB coatings on cobalt-based superalloy," *J Mater Res*, vol. 21, no. 3, pp. 737–746, Mar. 2006, doi: 10.1557/JMR.2006.0089/METRICS.

[9] **J. W. Lee and Y. C. Kuo,** "Cyclic oxidation behavior of a cobalt aluminide coating on Co-base superalloy AMS 5608," *Surf Coat Technol*, vol. 200, no. 5–6, pp. 1225–1230, Nov. 2005, doi: 10.1016/j.surfcoat.2005.07.082.

[10] **Y. Tamarin,** "Protective Coatings for Turbine Blades." Accessed: Jan. 08, 2025. [Online]. Available: https://www.amazon.com/Protective-Coatings-Turbine-Blades-Tamarin/dp/0871707594

[11] **A. J. McAlister,** "The Al-Co (Aluminum-Cobalt) system," *Bulletin of Alloy Phase Diagrams*, vol. 10, no. 6, pp. 646–650, Dec. 1989, doi: 10.1007/BF02877635/METRICS.

[12] **W. Shao, H. Hou, S. Liu, and J. LLorca,** "First-principles prediction of the Co–Al phase diagram including configurational, vibrational and magnetic contributions," *Journal of Materials Research and Technology*, vol. 31, pp. 1518–1534, Jul. 2024, doi: 10.1016/J.JMRT.2024.06.143.

[13] **R. Kossowsky and S. C. Singhal, Eds.,** "Surface Engineering," 1984, doi: 10.1007/978-94-009-6216-3.

[14] **Salvatore J. Grisaffe, Daniel L. Deadmore, William A. Sanders,** "Furnace and High-velocity Oxidation of Aluminide-coated Cobalt Superalloy WI-52 - - Google Kitaplar." Accessed: Apr. 20, 2025. [Online]. Available: https://books.google.com.tr/books?hl=tr&lr=&id=e6Brbm01jMoC&oi=fnd&pg=PA6&dq=WI-52+aluminide+coating&ots=1tygnAnqbw&sig=4rc4-yk_RMqctHY7N63IGB0lCYQ&redir_esc=y#v=onepage&q=WI-52%20aluminide%20coating&f=false

[15] **M. Yasin,** "Hot Corrosion Behavior of Modified Aluminide Coatngs on Cobalt-Base Superalloy," Jun. 1986.

[16] **W. BOESCH,** "Introduction—Superalloys," in *Superalloys Supercomposites Superceramics*, Elsevier, 1989, pp. 1–7. doi: 10.1016/b978-0-12-690845-9.50007-5.

[17] **F. C. Campbell,** "Superalloys," *Manufacturing Technology for Aerospace Structural Materials*, pp. 211–272, Jan. 2006, doi: 10.1016/B978-185617495-4/50006-8.

[18] **A. Kracke,** "Superalloys, the Most Successful Alloy System of Modern Times-Past, Present, and Future."

[19] **A. K. Jena and M. C. Chaturvedi,** "The role of alloying elements in the design of nickel-base superalloys," *J Mater Sci*, vol. 19, no. 10, pp. 3121–3139, Oct. 1984, doi: 10.1007/BF00549796/METRICS.

[20] **A. P. Mouritz,** *Introduction to Aerospace Materials*. Elsevier Inc., 2012. doi: 10.2514/4.869198.

[21] **Matthew J. Donachie, Stephen J. Donachie,** "Superalloys: A Technical Guide, 2nd Edition - - Google Kitaplar." Accessed: May 03, 2025. [Online]. Available: https://books.google.com.tr/books/about/Superalloys.html?id=vjCJ5pI1QpkC&redir_esc=y

[22] **Z. Zhang, H. Huang, Z. Zhang, Y. Wang, B. Zhu, and H. Zhao,** "A review of the microstructure and properties of superalloys regulated by magnetic field," *Journal of Materials Research and Technology*, vol. 30, pp. 9285–9317, May 2024, doi: 10.1016/J.JMRT.2024.05.189.

[23] **J. K. . Tien and Thomas. Caulfield,** *Superalloys, supercomposites, and superceramics*. Academic Press, 1989.

[24] **H. Farhat,** "Materials and coating technologies," *Operation, Maintenance, and Repair of Land-Based Gas Turbines*, pp. 63–87, Jan. 2021, doi: 10.1016/B978-0-12-821834-1.00007-1.

[25] **A. M. Beltran,** "Cobalt-base Alloys," in *Superalloys II*, 1987.

[26] **D. Coutsouradis, A. Davin, and M. Lamberigts,** "Cobalt-based superalloys for applications in gas turbines," *Materials Science and Engineering*, vol. 88, no. C, pp. 11–19, Apr. 1987, doi: 10.1016/0025-5416(87)90061-9.

[27] **İ. Can *et al.*,** "International Journal of Innovative Engineering Applications CFD ANALYSIS OF AN AIRCRAFT TURBOFAN ENGINE COMBUSTION PROCESS AND THE EFFECT ON TURBINE," *International Journal of Innovative Engineering Applications*, vol. 7, p. 1, 2023, doi: 10.46460/ijiea.1202422.

[28] **H. I. H. . Saravanamuttoo,** *Gas turbine theory*. Pearson, 2017.

[29] **J. R. Davis,** "ASM Specialty Handbook: Heat Resistant Materials," ® *ASM International*, vol. 3, p. 591, 2003, Accessed: May 03, 2025. [Online]. Available: https://www.asminternational.org/results/-/journal_content/56/16857762/PUBLICATION/

[30] **P. K. Domalavage,** "Process Development of Cobalt Base Superalloys Modified with Hafnium and Zirconium," Jun. 1980.

[31] **D. L. Klarstrom,** "Wrought cobalt- base superalloys," *J Mater Eng Perform*, vol. 2, no. 4, pp. 523–530, Aug. 1993, doi: 10.1007/BF02661736/METRICS.

[32] **W. Gui, H. Zhang, M. Yang, T. Jin, X. Sun, and Q. Zheng,** "The investigation of carbides evolution in a cobalt-base superalloy at elevated temperature," *J Alloys Compd*, vol. 695, pp. 1271–1278, 2017, doi: 10.1016/j.jallcom.2016.10.256.

[33] S. Michon, P. Berthod, L. Aranda, C. Rapin, R. Podor, and P. Steinmetz, "Application of thermodynamic calculations to study high temperature behavior of TaC-strengthened Co-base superalloys," *Calphad*, vol. 27, no. 3, pp. 289–294, Sep. 2003, doi: 10.1016/J.CALPHAD.2003.12.003.

[34] **C. Ling, S. Li, J. Hou, and H. Luo,** "Microstructure evolution and strengthening mechanism of carbides-reinforced Co–Cr–Nb–W alloy under high-temperature stress-rupture," *Materials Science and Engineering: A*, vol. 905, p. 145959, Jul. 2024, doi: 10.1016/J.MSEA.2023.145959.

[35] **W. Gui, H. Zhang, M. Yang, T. Jin, X. Sun, and Q. Zheng,** "Influence of type and morphology of carbides on stress-rupture behavior of a cast cobalt-base superalloy," *J Alloys Compd*, vol. 728, pp. 145–151, 2017, doi: 10.1016/j.jallcom.2017.08.287.

[36] **K. L. Luthra and J. H. Wood,** "High chromium cobalt-base coatings for low temperature hot corrosion," *Thin Solid Films*, vol. 119, no. 3, pp. 271–280, Sep. 1984, doi: 10.1016/0040-6090(84)90011-7.

[37] **A. Pakseresht and K. K. Amirtharaj Mosas, Eds.,** "Coatings for High-Temperature Environments," 2024, doi: 10.1007/978-3-031-45534-6.

[38] **R. Rajendran,** "Gas turbine coatings - An overview," Dec. 2012. doi: 10.1016/j.engfailanal.2012.07.007.

[39] **N. P. Padture, M. Gell, and E. H. Jordan,** "Thermal Barrier Coatings for Gas-Turbine Engine Applications Downloaded from," 2002. [Online]. Available: http://science.sciencemag.org/

[40] **R. Eriksson, K. Yuan, S. Johansson, R. L. Peng, and X. H. Li,** "Life Prediction of High-Temperature MCrAlY Coatings Based on Microstructural Observations," *Adv Mat Res*, vol. 922, pp. 143–148, 2014, doi: 10.4028/WWW.SCIENTIFIC.NET/AMR.922.143.

[41] **S. Bose,** "High Temperature Coatings," *High Temperature Coatings*, pp. 1–299, Jan. 2007, doi: 10.1016/B978-0-7506-8252-7.X5000-8.

[42] **D. K. Das, S. V. Joshi, and V. Singh,** "Evolution of aluminide coating microstructure on nickel-base cast superalloy CM-247 in a single-step high-activity aluminizing process," *Metallurgical and Materials Transactions A*, vol. 29, no. 8, pp. 2173–2188, 1998, Accessed: May 04, 2025. [Online]. Available: https://www.academia.edu/33727716/Evolution_of_aluminide_coating_microstructure_on_nickel_base_cast_superalloy_CM_247_in_a_single_step_high_activity_aluminizing_process

[43] **J. Jopek,** "High Temperature Protective Coatings for Aeroengine Applications," *MANUFACTURING TECHNOLOGY*, vol. 23, no. 4, 2023, doi: 10.21062/mft.2023.052.

[44] **J. M. N'Gandu-Muamba and R. Streiff,** "The reactive element effect (R.E.E.) : a tentative classification," *Journal de Physique IV Proceedings*, vol. 03, no. C9, pp. C9-281-C9-290, Dec. 1993, doi: 10.1051/JP4:1993927.

[45] **T. Roberts,** "The Structure and Stability of High Temperature Intermetallic Phases for Application within Coating Systems," 2009, *Cranfield University*. Accessed: Jan. 08, 2025. [Online]. Available: http://hdl.handle.net/1826/4499

[46] **S. Bose,** "OXIDATION- AND CORROSION-RESISTANT COATINGS," *High Temperature Coatings*, pp. 71–154, Jan. 2007, doi: 10.1016/B978-075068252-7/50007-X.

[47] **J. R. Nicholls, K. A. Long, and N. J. Simms,** "Diffusion Coatings," *Shreir's Corrosion*, pp. 2532–2555, Jan. 2010, doi: 10.1016/B978-044452787-5.00176-1.

[48] **R. Bianco and R. A. Rapp,** "Pack cementation diffusion coatings," *Metallurgical and Ceramic Protective Coatings*, pp. 236–260, 1996, doi: 10.1007/978-94-009-1501-5_9.

[49] **G. W. Goward and L. W. Cannon,** "Pack Cementation Coatings for Superalloys: A Review of History, Theory, and Practice," *J Eng Gas Turbine Power*, vol. 110, no. 1, pp. 150–154, Jan. 1988, doi: 10.1115/1.3240078.

[50] **X. Montero, M. C. Galetz, and M. Schütze,** "Low-activity aluminide coatings for superalloys using a slurry process free of halide activators and chromates," *Surf Coat Technol*, vol. 222, pp. 9–14, May 2013, doi: 10.1016/J.SURFCOAT.2013.01.033.

[51] **E. Pauletti and A. S. C. M. d'Oliveira,** "Study on the mechanisms of formation of aluminized diffusion coatings on a Ni-base superalloy using different pack aluminization procedures," *Journal of Vacuum Science & Technology A: Vacuum, Surfaces, and Films*, vol. 36, no. 4, Jul. 2018, doi: 10.1116/1.5026272.

[52] **M. Kopec,** "Citation: Kopec, M. Recent Advances in the Deposition of Aluminide Coatings on Nickel-Based Superalloys: A Synthetic Review Recent Advances in the Deposition of Aluminide Coatings on Nickel-Based Superalloys: A Synthetic Review (2019-2023)," 2019, doi: 10.3390/coatings14050630.

[53] **A. A. Inceyer, G. Güven, K. Demiralay, H. Kazdal Zeytin, and M. Usta,** "The Effects of Chemical Vapor Aluminizing Process Time and Post-processing for Nickel Aluminide Coating on CMSX-4 Alloy," *J Mater Eng Perform*, vol. 31, no. 3, pp. 2341–2353, Mar. 2022, doi: 10.1007/s11665-021-06323-w.

CURRICULUM VITAE

Name Surname **:** İlknur KARA

EDUCATION **:**

- **B.Sc.** **:** 2020, Istanbul University, Engineering Faculty, Metallurgical and Materials Engineering

PROFESSIONAL EXPERIENCE AND REWARDS:

- 2022- Materials and Special Process Engineer at BAYKAR TECHNOLOGIES
- 2021-2022 Quality Control Engineer at Ozdemir Model

PUBLICATIONS, PRESENTATIONS AND PATENTS ON THE THESIS:

- **Kara İ.,** Baydoğan M., Balcı E., "Effect of Homogenization Process on Microstructure of WI-52 Cobalt Based Superalloy" Dokuz Eylul University International Graduate Research Symposium (DEUIGRS'24), İzmir, Türkiye, 25-27 December 2024.